2-up-mix

NASA TECHNICAL NOTE

NASA TN D-7455

NASA TN D-7455

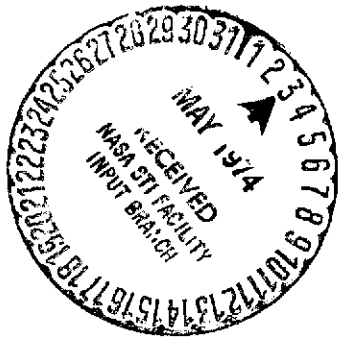

LATERAL STATIC AND DYNAMIC AERODYNAMIC PARAMETERS OF THE KESTREL AIRCRAFT (XV-6A) EXTRACTED FROM FLIGHT DATA

by William T. Suit and James L. Williams

Langley Research Center
Hampton, Va. 23665

NATIONAL AERONAUTICS AND SPACE ADMINISTRATION • WASHINGTON, D. C. • APRIL 1974

1. Report No.	2. Government Accession No.	3. Recipient's Catalog No.
NASA TN D-7455		

4. Title and Subtitle	5. Report Date
LATERAL STATIC AND DYNAMIC AERODYNAMIC PARAMETERS OF THE KESTREL AIRCRAFT (XV-6A) EXTRACTED FROM FLIGHT DATA	April 1974
	6. Performing Organization Code

7. Author(s)	8. Performing Organization Report No.
William T. Suit and James L. Williams	L-9176
	10. Work Unit No.
9. Performing Organization Name and Address	501-26-05-02
NASA Langley Research Center Hampton, Va. 23665	11. Contract or Grant No.
	13. Type of Report and Period Covered
12. Sponsoring Agency Name and Address	Technical Note
National Aeronautics and Space Administration Washington, D.C. 20546	14. Sponsoring Agency Code

15. Supplementary Notes

16. Abstract

Flight test data have been used to extract the lateral static and dynamic aerodynamic parameters of the Kestrel aircraft. The aircraft configurations included thrust-jet angles of 0°, 15°, and 30°, and the test Mach numbers were 0.43, 0.62, and 0.82. The results showed that most of the parameters varied linearly with trim normal-force coefficient. The directional stability parameter C_{n_β} showed a small increase with increasing trim normal-force coefficient and also with nozzle deflection. The effective-dihedral parameter C_{l_β}, the damping-in-roll parameter C_{l_p}, and damping-in-yaw parameter C_{n_r} all increased (became more negative) with increasing trim normal-force coefficient. For the latter three parameters, the effect of nozzle deflection was dependent on the trim normal-force coefficient.

17. Key Words (Suggested by Author(s))	18. Distribution Statement
Parameter extraction Maximum likelihood Aerodynamic coefficients	Unclassified – Unlimited STAR Category 02

19. Security Classif. (of this report)	20. Security Classif. (of this page)	21. No. of Pages	22. Price*
Unclassified	Unclassified	~~42~~ 45	$3.25

*For sale by the National Technical Information Service, Springfield, Virginia 22151

LATERAL STATIC AND DYNAMIC AERODYNAMIC PARAMETERS OF THE KESTREL AIRCRAFT (XV-6A) EXTRACTED FROM FLIGHT DATA

By William T. Suit and James L. Williams
Langley Research Center

SUMMARY

A maximum likelihood extraction method has been used to extract the lateral static and dynamic aerodynamic parameters of the Kestrel aircraft from flight test data. The aircraft configurations included thrust-jet angles of 0°, 15°, and 30°, and the test Mach numbers were 0.43, 0.62, and 0.82. The results showed that most of the parameters varied linearly with trim normal-force coefficient. The directional stability parameter C_{n_β} showed a small increase with increasing trim normal-force coefficient and also with nozzle deflection. The effective-dihedral parameter C_{l_β}, the damping-in-roll parameter C_{l_p}, and damping-in-yaw parameter C_{n_r} all increased (became more negative) with increasing trim normal-force coefficient. For the latter three parameters, the effect of nozzle deflection was dependent on the trim normal-force coefficient.

INTRODUCTION

Analytical and simulator studies of the flight and handling qualities of aircraft require that accurate estimates of the aerodynamic parameters be used if the results are to be valid. There are several methods of obtaining the parameters. These include methods presented in various books, wind-tunnel tests, and extraction of derivatives from flight test data. Of these methods, derivatives determined from flight tests should be the most accurate since the results are obtained with the aircraft in its proper environment.

To provide aerodynamic parameters that were difficult to determine by other methods, parameters have been extracted from flight data for many years. In the past, many of the attempts yielded unacceptable results. At present, improvements in

instrumentation and particularly the development of large capacity high-speed computers enable the engineer to take advantage of the advanced mathematical methods of parameter extraction. Example results from recent studies made at the Langley Research Center by using an advanced extraction method are reported in references 1 to 4.

The purpose of the present study is to determine the lateral aerodynamic parameters of the Kestrel aircraft from flight data for several airspeeds and thrust vector angles. The technique and program used in extracting the parameters is that of reference 5.

SYMBOLS

Values are given in both SI and U.S. Customary Units. The measurements and calculations were made in U.S. Customary Units.

a	acceleration, m/sec^2 (ft/sec^2)
b	wing span, m (ft)
F_j	primary engine thrust, N (lb)
F_Y	aerodynamic forces along aircraft Y-axis, N (lb)
F_Z	aerodynamic forces along aircraft Z-axis, N (lb)
g	acceleration due to gravity, $1g = 9.81\ m/sec^2$ $(32.2\ ft/sec^2)$
h	altitude, m (ft)
I	moment of inertia, $kg\text{-}m^2$ $(slug\text{-}ft^2)$
M	Mach number
M_X	moment about X body axis, N-m (ft-lb)

$M_{X,j}$ rolling moment due to reaction jets, N-m (ft-lb)

M_Z moment about Z body axis, N-m (ft-lb)

$M_{Z,j}$ yawing moment due to reaction jets, N-m (ft-lb)

N_f engine fan speed, percent of maximum speed

p rate of roll, rad/sec or deg/sec

q rate of pitch, rad/sec

$\bar{q}$ dynamic pressure, $\frac{1}{2}\rho V^2$, Pa (lbf/ft^2)

r rate of yaw, rad/sec or deg/sec

S total wing area, m^2 (ft^2)

u velocity along X body axis, m/sec (ft/sec)

V aircraft total velocity, m/sec (ft/sec)

v velocity along Y body axis, m/sec (ft/sec)

W aircraft weight, N (lb)

w velocity along Z body axis, m/sec (ft/sec)

X_i individual state in complete state vector X

α angle of attack, rad or deg

β angle of sideslip, rad

δ_a differential aileron deflection (positive for right aileron up), rad or deg

δ_r rudder deflection (positive for trailing edge right), rad or deg

θ pitch angle, rad

θ_j jet nozzle angle, deg

ρ air density, kg/m^3 $(slugs/ft^3)$

ϕ roll angle, rad

C_l rolling-moment coefficient, $\frac{M_X}{\frac{1}{2}\rho V^2 Sb}$

C_n yawing-moment coefficient, $\frac{M_Z}{\frac{1}{2}\rho V^2 Sb}$

C_T thrust coefficient, $\frac{F_j}{\frac{1}{2}\rho V^2 S}$

C_Y side-force coefficient, $\frac{F_Y}{\frac{1}{2}\rho V^2 S}$

C_Z normal-force coefficient, $\frac{F_Z}{\frac{1}{2}\rho V^2 S}$

$C_{l_p} = \frac{\partial C_l}{\partial \frac{pb}{2V}}$

$C_{l_r} = \frac{\partial C_l}{\partial \frac{rb}{2V}}$

$C_{l_\beta} = \frac{\partial C_l}{\partial \beta}$

$C_{l_{\delta_a}} = \frac{\partial C_l}{\partial \delta_a}$

$$C_{l_{\delta_r}} = \frac{\partial C_l}{\partial \delta_r}$$

$$C_{n_p} = \frac{\partial C_n}{\partial \frac{pb}{2V}}$$

$$C_{n_r} = \frac{\partial C_n}{\partial \frac{rb}{2V}}$$

$$C_{n_\beta} = \frac{\partial C_n}{\partial \beta}$$

$$C_{n_{\delta_a}} = \frac{\partial C_n}{\partial \delta_a}$$

$$C_{n_{\delta_r}} = \frac{\partial C_n}{\partial \delta_r}$$

$$C_{Y_p} = \frac{\partial C_Y}{\partial \frac{pb}{2V}}$$

$$C_{Y_r} = \frac{\partial C_Y}{\partial \frac{rb}{2V}}$$

$$C_{Y_\beta} = \frac{\partial C_Y}{\partial \beta}$$

$$C_{Y_{\delta_r}} = \frac{\partial C_Y}{\partial \delta_r}$$

Subscripts:

c computed

m measured

o indicates coefficient at trim conditions

t indicates state at trim conditions

X X-axis

Y Y-axis

Z Z-axis

A dot over a symbol signifies a derivative with respect to time.

The following symbols are used only in figures 4 to 6 and result from the limitations of the computer-controlled plotting equipment:

AYI lateral acceleration, m/sec^2 (ft/sec^2)

$DA = \delta_a - \delta_{a,t}$, rad

$DR = \delta_r - \delta_{r,t}$, rad

P roll rate, rad/sec

PHI roll attitude, rad

R yaw rate, rad/sec

V lateral velocity, m/sec (ft/sec)

EQUATIONS OF MOTION

The equations of motion used in this study are referred to a body-axis system and are as follows:

Y-direction:

$$\dot{v} = pw - ru + g \cos\theta \sin\phi + \frac{1}{2}\rho V^2 S \frac{g}{W}\left[C_{Y,o} + C_{Y_\beta}\beta + C_{Y_p}\frac{pb}{2V} + C_{Y_r}\frac{rb}{2V} + C_{Y_{\delta_r}}\left(\delta_r - \delta_{r,t}\right)\right] \quad (1)$$

Rolling moment:

$$\dot{p} = \frac{I_{XZ}}{I_X}\dot{r} + \frac{I_Y - I_Z}{I_X}qr + \frac{I_{XZ}}{I_X}pq + \frac{M_{X,j}}{I_X} + \frac{1}{2}\frac{\rho V^2 Sb}{I_X}\left[C_{l,o} + C_{l_\beta}\beta + C_{l_p}\frac{pb}{2V} + C_{l_r}\frac{rb}{2V} + C_{l_{\delta_r}}\left(\delta_r - \delta_{r,t}\right) + C_{l_{\delta_a}}\left(\delta_a - \delta_{a,t}\right)\right] \quad (2)$$

Yawing moment:

$$\dot{r} = \frac{I_{XZ}}{I_Z}\dot{p} + \frac{I_X - I_Y}{I_Z}pq - \frac{I_{XZ}}{I_Z}qr + \frac{M_{Z,j}}{I_Z} + \frac{1}{2}\frac{\rho V^2 Sb}{I_Z}\left[C_{n,o} + C_{n_p}\frac{pb}{2V} + C_{n_r}\frac{rb}{2V} + C_{n_{\delta_r}}\left(\delta_r - \delta_{r,t}\right) + C_{n_{\delta_a}}\left(\delta_a - \delta_{a,t}\right)\right] \quad (3)$$

TEST AIRCRAFT AND EQUIPMENT

The test aircraft used in this flight investigation was a Hawker Siddeley Kestrel (XV-6A). The Kestrel is a single-place, prototype, vectored-thrust, V/STOL strike-reconnaissance aircraft. A three-view drawing of the aircraft is shown as figure 1.

A single Rolls-Royce Bristol Pegasus 5 turbofan engine powers the Kestrel. The Pegasus is an axial-flow, vectored-exhaust turbofan engine, with a 1.4 bypass ratio, having an uninstalled sea-level static thrust rating of 68 900 N (15 500 lb). Thrust is

vectored through two pairs of controllable engine exhaust nozzles (shown in fig. 1) and is equally distributed between the forward nozzles which exhaust bypass air from the fan and the aft nozzles which exhaust turbine air. The nozzles are mechanically interconnected and can be rotated at rates up to 90 deg/sec to any position from fully aft ($\theta_j = 0^o$) to 5^o forward of vertically downward ($\theta_j = 95^o$). Nozzle angle is controlled by a single lever which is located inboard on the throttle quadrant and which is the only additional control required for thrust vectoring in the Kestrel.

Control moments during nonvectored flight are provided by conventional aerodynamic surfaces. The ailerons and tail plane are powered by tandem hydraulic systems; the rudder is unpowered.

During vectored flight, reaction control moments are added to those produced by the normal aerodynamic surfaces. Reaction control shutter valves, located at the nose, tail, and wing tips, are mechanically connected to their corresponding aerodynamic control surface and receive high-pressure engine bleed air as a function of engine nozzle angle. (See fig. 1.) Full reaction control is provided at engine nozzle angles greater than 30^o. No stability augmentation system (SAS) is provided. However, during flight at low dynamic pressures where the pilot does not get feedback to the control stick from forces on the control surfaces, an artificial-feel system is provided. Lateral feel is provided by a nonlinear spring unit and longitudinal forces are provided by a g-feel unit supplemented with a feel spring. This g-feel unit is a bobweight in the control run which increases longitudinal maneuvering forces by 8.9 N/g (2 lb/g) for normal acceleration and $4.9 \frac{N}{rad/sec^2} \left(1.1 \frac{lb}{rad/sec^2}\right)$ for pitch acceleration.

The rolling and yawing moments due to the reaction jets are given by the following empirical equations which were obtained from the manufacturer:

$$M_{X,j} = \left[1 - 2.14\left(1 - \frac{N_f}{100}\right)\right] \left|\frac{\theta_j}{20}\right| M_{X,j}'$$

$$M_{Z,j} = \left[1 - 2.14\left(1 - \frac{N_f}{100}\right)\right] \left|\frac{\theta_j}{20}\right| M_{Z,j}'$$

where

$$\left|\frac{\theta_j}{20}\right| = 1 \quad \text{for} \quad \theta_j \geq 20$$

and where $M_{X,j}'$ and $M_{Z,j}'$ are taken from figures 2 and 3, respectively. The information for figures 2 and 3 was taken from a manufacturer's report at the time of the problem setup. Modifications to the aircraft probably have resulted in a different reaction jet curve. Since the reaction jets are not particularly effective (in comparison with the aerodynamic controls) over the test Mach number range, any differences that exist were not considered significant. Additional aircraft and engine data are presented in table I.

FLIGHT TESTS

The aircraft was flown at nominal Mach numbers of 0.82, 0.62, and 0.43 with three nozzle deflections, 0°, 15°, and 30°, and at constant thrust for each flight condition. The altitude for the flights was about 4.6 km (15 000 ft). At each nozzle deflection and airspeed several runs were made with the pilot perturbing the aircraft from a 1g level flight condition with different combinations of aileron and rudder inputs. The pilots were instructed to exercise the rudder and ailerons by means of successive inputs in both the positive and negative senses. The form of the inputs was generally left to the pilot but he was instructed that, if possible, some of the inputs should be abrupt. Flight test conditions are given in table II.

For the purpose of this analysis, the center of gravity was assumed to be at 13.7 percent wing mean aerodynamic chord, and the average values of weights and inertias listed in table I were used. Data pertinent to this study were recorded during flight tests. The recorded quantities which were used are listed in table III. The full-scale range of the recording instruments and their response frequency are also given in table III. A filter was used to limit the response frequency of the instruments. In general, the instruments had responses which were flat past the filter frequency. The accuracy of these measurements was estimated to be 3 percent on full scale for the states measured. The α and β vanes used in this investigation were located on a nose boom approximately 1.8 m (6 ft) in front of the aircraft. The vanes were made of balsa wood and the error introduced by the vanes themselves was small compared to the estimated accuracy of 3 percent of full scale. The readings from the α and β vanes were corrected for the effects of angular rates.

PARAMETER-EXTRACTION TECHNIQUE

All the data were stored on an onboard magnetic tape recorder by using wide-band FM recording techniques. The linear velocities along the vehicle body axes were calculated from the measured airspeed, angle of attack, and angle of sideslip. The corrected and calculated data were put on a tape for use in the parameter-extraction program at a rate of 20 points per second. Additional details on preparation of flight data for the extraction program are given in reference 1.

The parameter-estimation procedure used in this study is an iterative procedure which maximizes the conditional likelihood function L. This L is a function of the aerodynamic parameters, weights, and initial conditions given by the relation

$$L = \frac{1}{(2\pi)^{1/2}|R|^{1/2}} \exp\left\{-\frac{1}{2}\sum_{i=1}^{N}\left[(X_i)_m - (X_i)_c\right]^T R^{-1}\left[(X_i)_m - (X_i)_c\right]\right\}$$

where N is the number of data points, R is the estimate of the error covariance matrix, $(X_i)_m$ is a vector quantity whose elements are the measured states, and $(X_i)_c$ is a vector of the calculated states whose elements are determined from the integration of equations (1) to (3). Maximizing the likelihood function minimizes the difference between the measured and calculated aircraft motions $\left[(X_i)_m - (X_i)_c\right]$. A detailed description of the method used is given in reference 5.

The states used in the likelihood function were v, p, r, and a_Y. In this study the initial values of v, p, r, and a_Y were not estimated. The aircraft was initially in trimmed, level flight and the initial values of v, p, r, and a_Y were assumed to be zero; the flight data were biased so that v, p, r, and a_Y were initially as close to zero as possible. An average of the first three data points was used as the initial estimated point.

After convergence of the likelihood function was established for a given flight data record, the extracted aerodynamic derivatives were examined. The derivatives were accepted as well determined if (a) the standard deviations of the computed time histories of the aircraft motion from the measured time histories, as given by equation (4) in the subsequent section, were less than the measurement uncertainties, (b) the change in derivatives was small for successive iterations, and (c) the standard deviation of each derivative was less than about one-tenth of the extracted value of the derivative. In some

cases, parameter values were accepted which had standard deviations greater than 10 percent of the parameter value. These parameters were not considered well determined, but were the best values obtainable for the particular mathematical model and set of flight data used in this investigation.

RESULTS AND DISCUSSION

Presentation of Data

Data for the flight conditions listed in table II were used to determine a set of aerodynamic derivatives for each of the flight conditions. Sample measured and computed time histories for each flight condition are shown in figures 4 to 6. The maximum number of points available for any run was 300; however, a reduced number of the flight data points were plotted to make the figures more readable. The scales used for the different states in figures 4 to 6 were determined to give maximum definition for each state and, therefore, the scales are not uniform run to run. The figures show that in all cases the computed time histories were generally in close agreement with the flight records. Table IV gives the standard deviations of the computed states from the measured states which are given by the expression:

$$\text{Standard deviation} = \left\{ \frac{1}{N} \sum_{i=1}^{N} \left[(X_i)_m - (X_i)_c \right]^T \left[(X_i)_m - (X_i)_c \right] \right\}^{1/2} \tag{4}$$

where N is the number of data points. The derivatives extracted for each flight condition (the derivatives which resulted in the computed time histories of figs. 4 to 6) are listed in table V along with their standard deviations.

The time histories shown were used to determine the majority of the parameter values and standard deviations presented in table V. However, since the time histories presented are only a representative sample of all the data examined, some of the numbers shown in table V came from runs other than those shown as figures 4 to 6. In some cases there was not sufficient information in the data to determine particular derivatives (for example, δ_r derivatives for the $M = 0.43$, $\theta_j = 15^\circ$ and 30° cases). In these cases the best determined number from other runs at similar flight conditions was used. In all cases the fit to the measured data shown in figures 4 to 6 was for the numbers given in table V.

Discussion of Results

Some of the aerodynamic coefficients listed in table V may vary with changes in Mach number, angle of attack, and thrust coefficient. The individual effects of the factors listed on particular parameters are difficult to determine. The trim normal-force coefficient $C_{Z,o}$ includes the effects of Mach number, angle of attack, and thrust coefficient. Thus, by plotting the coefficients of table V against trim normal-force coefficient, the effect of a combined variation of factors can be presented.

Sideslip derivatives.- The directional stability parameter C_{n_β} generally shows a small increase with trim normal-force coefficient for a given nozzle deflection (fig. 7(a)). The data also indicate an increase in directional stability with increasing nozzle deflection for the range of flight conditions of this study. Figure 22 of reference 6 shows that for the C_T range of the present study ($C_T = 0.121$ to $C_T = 0.196$) only a small change in sideslip derivatives would be expected. Although the wind-tunnel test conditions of reference 6 are not closely comparable to those of the present study, reference 6 indicates greater directional stability than does the present study.

The effective-dihedral parameter C_{l_β} increases (becomes more negative) with trim normal-force coefficient for all nozzle settings of this study. Although the effect of nozzle deflection is not clearly defined, it does depend on trim normal-force coefficient. The parameter C_{Y_β} was not well determined (standard deviation greater than 10 percent) for the data used in this investigation and did not show definite trends with trim normal-force coefficient or nozzle angle.

Rolling derivatives.- The damping-in-roll parameter C_{l_p} generally increased (became more negative) with increase in trim normal-force coefficient for any given nozzle deflection (fig. 7(b)). The effect of nozzle deflection depends on the trim normal-force coefficient. The parameter C_{n_p} generally becomes more negative with increase in normal-force coefficient for a given nozzle deflection. There is a large negative increase in C_{n_p} when the nozzle deflection is changed from 0^o to 15^o; however, larger nozzle deflections have no appreciable effect on C_{n_p}. The parameters C_{n_p} and C_{Y_p} were not as well defined as C_{l_p} and they exhibited a more erratic variation with $C_{Z,o}$.

Yawing derivatives.- The damping-in-yaw parameter C_{n_r} generally increases (becomes more negative) with increase in normal-force coefficient for a given nozzle deflection (fig. 7(c)). The effect of nozzle deflection is not clearly defined, although it

does depend on trim normal-force coefficient. The parameter C_{l_r} shows a nonlinear variation with normal-force coefficient. However, C_{l_r} and C_{Y_r} were not as well determined as C_{n_r}.

Control derivatives.- The control derivatives $C_{l_{\delta_a}}$ and $C_{n_{\delta_r}}$ generally show a small increase with normal-force coefficient, and no appreciable change with nozzle deflection (figs. 7(d) and (e)). The other control derivatives $C_{Y_{\delta_r}}$, $C_{l_{\delta_r}}$, and $C_{n_{\delta_a}}$ are not as well defined.

The trim coefficients $C_{Y,o}$, $C_{l,o}$, and $C_{n,o}$ should have had values of zero if the aircraft was completely trimmed before it was perturbed. The nonzero values for the trim coefficients reflect the fact that the aircraft was not completely trimmed and that there were biases in the data that were not accounted for.

In general, the extracted parameters which were well defined showed consistent and repeatable results for all runs. The parameters which were not well defined showed a more erratic behavior as has been noted in the preceding discussion, although the values obtained for these parameters were not unreasonable. For the well-defined parameters the data indicate that for each θ_j, the parameters vary linearly with trim normal-force coefficient. Although the aerodynamic parameters appear to have a linear variation with normal-force coefficient for the flight data examined in this investigation, in general, some nonlinearity due to Mach number could be expected at the highest Mach number.

CONCLUDING REMARKS

Flight test data have been used to extract the lateral static and dynamic aerodynamic parameters of the Kestrel aircraft. The aircraft configurations included thrust-jet angles of 0°, 15°, and 30°, and the test Mach numbers were 0.43, 0.62, and 0.82. The following parameters were considered to have been determined better than the other parameters: effective-dihedral parameter C_{l_β}, damping-in-roll parameter C_{l_p}, aileron effectiveness parameter $C_{l_{\delta_a}}$, directional stability parameter C_{n_β}, damping-in-yaw parameter C_{n_r}, and rudder effectiveness parameter $C_{n_{\delta_r}}$. The results showed that these parameters varied linearly with trim normal-force coefficient. The directional stability parameter C_{n_β} showed a small increase with increasing trim normal-force coefficient

and also with nozzle deflection. The effective-dihedral parameter C_{l_β}, the damping-in-roll parameter C_{l_p}, and damping-in-yaw parameter C_{n_r} all increased (became more negative) with increasing trim normal-force coefficient. For the latter three parameters, the effect of nozzle deflection was dependent on the trim normal-force coefficient.

Langley Research Center,
National Aeronautics and Space Administration,
Hampton, Va., December 17, 1973.

REFERENCES

1. Suit, William T.: Aerodynamic Parameters of the Navion Airplane Extracted From Flight Data. NASA TN D-6643, 1972.

2. Steinmetz, George C.; Parrish, Russell V.; and Bowles, Roland L.: Longitudinal Stability and Control Derivatives of a Jet Fighter Airplane Extracted From Flight Test Data by Utilizing Maximum Likelihood Estimation. NASA TN D-6532, 1972.

3. Williams, James L.: Extraction of Longitudinal Aerodynamic Coefficients From Forward-Flight Conditions of a Tilt-Wing V/STOL Airplane. NASA TN D-7114, 1972.

4. Suit, William T.; and Williams, James L.: Longitudinal Aerodynamic Parameters of the Kestrel Aircraft (XV-6A) Extracted From Flight Data. NASA TN D-7296, 1973.

5. Grove, Randall D.; Bowles, Roland L.; and Mayhew, Stanley C.: A Procedure for Estimating Stability and Control Parameters From Flight Test Data by Using Maximum Likelihood Methods Employing a Real-Time Digital System. NASA TN D-6735, 1972.

6. Margason, Richard J.; Vogler, Raymond D.; and Winston, Matthew M.: Wind-Tunnel Investigation at Low Speeds of a Model of the Kestrel (XV-6A) Vectored-Thrust V/STOL Airplane. NASA TN D-6826, 1972.

TABLE I.- GENERAL AIRCRAFT AND ENGINE DATA

Weights:	
Empty weight, N (lb)	45 370 (10 200)
Design gross weight, N (lb)	78 280 (17 600)
Maximum hovering weight, N (lb)	57 820 (13 000)
Total internal fuel, N (lb)	22 240 (5 000)
Moments of inertia at 61 340 N (13 790 lbf):	
I_{ZZ}, kg-m^2 (slug-ft^2)	33 200 (24 500)
I_{YY}, kg-m^2 (slug-ft^2)	30 490 (22 500)
I_{XX}, kg-m^2 (slug-ft^2)	5 420 (4 000)
I_{XZ}, kg-m^2 (slug-ft^2)	2 300 (1 700)
Fuselage:	
Length, m (ft)	12.97 (42.54)
Height to top of vertical tail, m (ft)	3.28 (10.75)
Wetted area, net, m^2 (ft^2)	45.99 (495.0)
Wing:	
Area, total, m^2 (ft^2)	17.32 (186.4)
Area, exposed, m^2 (ft^2)	12.27 (132.1)
Span, m (ft)	6.98 (22.9)
Mean aerodynamic chord, m (in.)	2.49 (98.0)
Dihedral angle, deg	-12.0
Taper ratio	0.40
Aspect ratio	2.8
Sweepback of leading edge, deg	40.0
Aileron area, m^2 (ft^2)	0.98 (10.54)
Left-aileron travel limits:	
Trailing edge full down, deg	12.0
Trailing edge full up, deg	13.0
Trim range, deg	±3.5
Flap area (left and right), m^2 (ft^2)	1.23 (13.25)
Flap travel limit, deg	50
Tail plane:	
Area, gross, m^2 (ft^2)	4.41 (47.5)
Area, net, m^2 (ft^2)	3.84 (41.3)
Span, m (ft)	4.24 (13.92)
Aspect ratio	3.26
Dihedral angle, deg	-15.5
Standard mean chord, m (ft)	1.04 (3.41)
Tail-plane travel limits:	
Trailing edge full down, deg	11.5
Trailing edge full up, deg	10.0
Trim range, deg	7.5 to -3.5

TABLE I.- GENERAL AIRCRAFT AND ENGINE DATA – Concluded

Vertical tail:		
Area, gross, m^2 (ft^2)	2.42	(26.1)
Aspect ratio	1.22	
Rudder area, m^2 (ft^2)	0.509	(5.48)
Rudder travel limits:		
Trailing edge left and right, deg	15.0	
Trim tab movement, deg	±5.0	
Reaction control system:		
Full nose-up reaction pitch control at tail-plane angle, deg	4.5	
Full pitch control, tail plane, deg	10.0	
Full roll control, aileron (total), deg	±14	
Full yaw control, rudder, deg	±10	
Pitch reaction control arm about center of gravity:		
Pitch nose-up, m (ft)	4.62	(15.15)
Pitch nose-down, m (ft)	7.26	(23.83)
Roll reaction arm about center line, m (ft)	3.39	(11.12)
Yaw reaction arm about center of gravity, m (ft)	7.08	(23.24)
Engine data:		
Number and model	Rolls-Royce Bristol Pegasus 5	
Type	Ducted-fan lift-thrust engine	
Intake area, m^2 (ft^2)	0.86	(9.3)
Bypass ratio	1.4	
Maximum thrust, uninstalled sea level, N (lb)	68 900	(15 500)

Operating limitations:

Power rating	Reaction control bleed	N_f, percent	Exhaust gas temperature, ^oC	Time limit
Maximum	With bleed	93.5	645	2.5 min
	No bleed	93.5	595	2.5 min
Maximum continuous	With bleed	85.0	540	Unlimited
	No bleed	89.0	540	Unlimited

TABLE II.- FLIGHT TEST CONDITIONS

Nozzle angle, θ, deg	Mach number	N_f, percent	F_j	
			N	lbf
0	0.82	85	55 200	12 400
0	.62	75	33 000	7 400
0	.43	65	20 000	4 500
15	.82	86	57 800	13 000
15	.62	76	34 000	7 700
15	.43	67	23 000	5 100
30	.82	89	62 000	14 000
30	.43	71	25 000	5 600

TABLE III.- RANGES AND FREQUENCY RESPONSE OF INSTRUMENTS

State	Range	Frequency response, Hz
a_Y	±2g	6
V	0 to 366 m/sec (0 to 1200 ft/sec)	2
θ	±60°	4
ϕ	±120°	4
q	±45 deg/sec	6
r	±45 deg/sec	6
p	±60 deg/sec	6
α	-10° to 30°	4
β	±20°	4
h	0 to 18.29 km (0 to 60 000 ft)	2
δ_a	±12.5°	4
δ_r	±15°	4

TABLE IV.- STANDARD DEVIATIONS OF THE CALCULATED RELATIVE STATES FROM THE MEASURED STATES AT CONVERGENCE

State	Standard deviations for nozzle angles of –								
	0^o			15^o			30^o		
	M = 0.82	M = 0.62	M = 0.43	M = 0.82	M = 0.62	M = 0.43	M = 0.82	M = 0.62	M = 0.43
v	0.84 m/sec (2.75 ft/sec)	0.49 m/sec (1.61 ft/sec)	0.42 m/sec (1.39 ft/sec)	0.55 m/sec (1.81 ft/sec)	0.64 m/sec (2.09 ft/sec)	0.67 m/sec (2.21 ft/sec)	1.01 m/sec (3.33 ft/sec)	No data available	0.31 m/sec (1.01 ft/sec)
p	2.59 deg/sec	1.39 deg/sec	2.50 deg/sec	2.11 deg/sec	1.46 deg/sec	2.11 deg/sec	2.81 deg/sec		1.48 deg/sec
r	0.46 deg/sec	0.31 deg/sec	0.43 deg/sec	0.37 deg/sec	0.31 deg/sec	0.27 deg/sec	0.41 deg/sec		0.19 deg/sec
a_Y	0.27 m/sec^2 (0.88 ft/sec^2)	0.15 m/sec^2 (0.50 ft/sec^2)	0.13 m/sec^2 (0.44 ft/sec^2)	0.16 m/sec^2 (0.54 ft/sec^2)	0.21 m/sec^2 (0.68 ft/sec^2)	0.12 m/sec^2 (0.38 ft/sec^2)	0.26 m/sec^2 (0.86 ft/sec^2)		0.12 m/sec^2 (0.38 ft/sec^2)

TABLE V.- EXTRACTED AERODYNAMIC PARAMETERS AND STANDARD DEVIATIONS

Parameter	Extracted aerodynamic parameters and standard deviations for –							
	$\theta_j = 0^o$ $M \approx 0.82$ $\bar{q} = 27.53$ kPa (575 lbf/ft^2) $C_T = 0.121$ $\alpha = 1.75^o$	$\theta_j = 0^o$ $M \approx 0.62$ $\bar{q} = 15.42$ kPa (322 lbf/ft^2) $C_T = 0.121$ $\alpha = 3.33^o$	$\theta_j = 0^o$ $M \approx 0.43$ $\bar{q} = 7.517$ kPa (157 lbf/ft^2) $C_T = 0.155$ $\alpha = 8.94^o$	$\theta_j = 15^o$ $M \approx 0.82$ $\bar{q} = 27.53$ kPa (575 lbf/ft^2) $C_T = 0.1195$ $\alpha = 0.722^o$	$\theta_j = 15^o$ $M \approx 0.62$ $\bar{q} = 15.42$ kPa (322 lbf/ft^2) $C_T = 0.128$ $\alpha = 4.70^o$	$\theta_j = 15^o$ $M \approx 0.43$ $\bar{q} = 7.517$ kPa (157 lbf/ft^2) $C_T = 0.137$ $\alpha = 8.10^o$	$\theta_j = 30^o$ $M \approx 0.82$ $\bar{q} = 27.53$ kPa (575 lbf/ft^2) $C_T = 0.139$ $\alpha = 0.653^o$	$\theta_j = 30^o$ $M \approx 0.43$ $\bar{q} = 7.517$ kPa (157 lbf/ft^2) $C_T = 0.196$ $\alpha = 7.91^o$
$C_{Y,o}$	-0.00061 ± 0.00034	-0.00023 ± 0.00033	0.018 ± 0.0006	0.0017 ± 0.00022	-0.0027 ± 0.00045	-0.0073 ± 0.00073	-0.00081 ± 0.00046	0.00021 ± 0.00073
C_{Y_β}	-0.743 ± 0.63	-1.09 ± 0.52	-1.44 ± 0.65	-0.97 ± 0.047	-1.08 ± 0.056	-1.5 ± 0.14	-1.36 ± 0.078	-1.11 ± 0.16
C_{Y_p}	0.775 ± 0.33	0.13 ± 0.18	0.78 ± 0.21	0.67 ± 0.17	-0.12 ± 0.15	1.19 ± 0.17	-0.13 ± 0.17	1.14 ± 0.23
C_{Y_r}	6.54 ± 1.19	4.3 ± 1.04	3.1 ± 1.16	1.56 ± 0.83	1.1 ± 0.93	1.1 ± 0.82	4.0 ± 1.2	-2.11 ± 0.63
$C_{Y_{\delta_r}}$	-0.153 ± 0.044	-0.24 ± 0.046	-0.34 ± 0.075	-0.135 ± 0.036	-0.226 ± 0.06	-0.19 ± 0.046	-0.12 ± 0.082	-0.12 ± 0.047
$C_{l,o}$	-0.00005 ± 0.000013	-0.000023 ± 0.000015	0.00024 ± 0.000035	-0.0000018 ± 0.000011	-0.00013 ± 0.00002	0.00061 ± 0.000067	-0.000092 ± 0.000023	-0.00032 ± 0.00003
C_{l_β}	-0.044 ± 0.0046	-0.084 ± 0.0031	-0.15 ± 0.0045	-0.056 ± 0.005	-0.081 ± 0.0027	-0.19 ± 0.0037	-0.081 ± 0.0061	-0.10 ± 0.008
C_{l_p}	-0.166 ± 0.016	-0.22 ± 0.012	-0.21 ± 0.015	-0.13 ± 0.014	-0.21 ± 0.009	-0.29 ± 0.016	-0.16 ± 0.015	-0.26 ± 0.009
C_{l_r}	0.53 ± 0.067	0.19 ± 0.050	0.32 ± 0.061	0.19 ± 0.05	0.06 ± 0.031	0.83 ± 0.071	0.54 ± 0.059	0.20 ± 0.04
$C_{l_{\delta_r}}$	-0.017 ± 0.003	-0.028 ± 0.003	-0.049 ± 0.005	-0.019 ± 0.003	-0.025 ± 0.003	-0.020 ± 0.003	-0.025 ± 0.006	-0.020 ± 0.0035
$C_{l_{\delta_a}}$	0.025 ± 0.0035	0.044 ± 0.0034	0.05 ± 0.0042	0.023 ± 0.004	0.032 ± 0.002	0.049 ± 0.005	0.022 ± 0.0045	0.035 ± 0.002
$C_{n,o}$	0.00024 ± 0.000036	0.00015 ± 0.000027	0.00027 ± 0.000042	-0.000203 ± 0.000026	0.000486 ± 0.000037	-0.00065 ± 0.000067	0.00021 ± 0.000055	0.00096 ± 0.000047
C_{n_β}	0.15 ± 0.002	0.15 ± 0.0013	0.175 ± 0.0033	0.18 ± 0.0018	0.17 ± 0.0011	0.21 ± 0.007	0.20 ± 0.003	0.26 ± 0.007
C_{n_p}	0.048 ± 0.014	-0.015 ± 0.009	-0.052 ± 0.011	-0.094 ± 0.017	-0.071 ± 0.007	-0.22 ± 0.019	-0.067 ± 0.017	-0.17 ± 0.018
C_{n_r}	-0.63 ± 0.042	-0.84 ± 0.044	-1.01 ± 0.053	-0.69 ± 0.056	-0.71 ± 0.035	-0.76 ± 0.051	-0.95 ± 0.078	-1.12 ± 0.04
$C_{n_{\delta_r}}$	0.062 ± 0.0024	0.090 ± 0.0024	0.14 ± 0.0044	0.064 ± 0.0026	0.082 ± 0.0024	0.12 ± 0.005	0.062 ± 0.0049	0.12 ± 0.0051
$C_{n_{\delta_a}}$	0.007 ± 0.0019	0.012 ± 0.0021	0.008 ± 0.0034	0.005 ± 0.0022	0.010 ± 0.0014	0.020 ± 0.0045	0.018 ± 0.0032	0.007 ± 0.0027

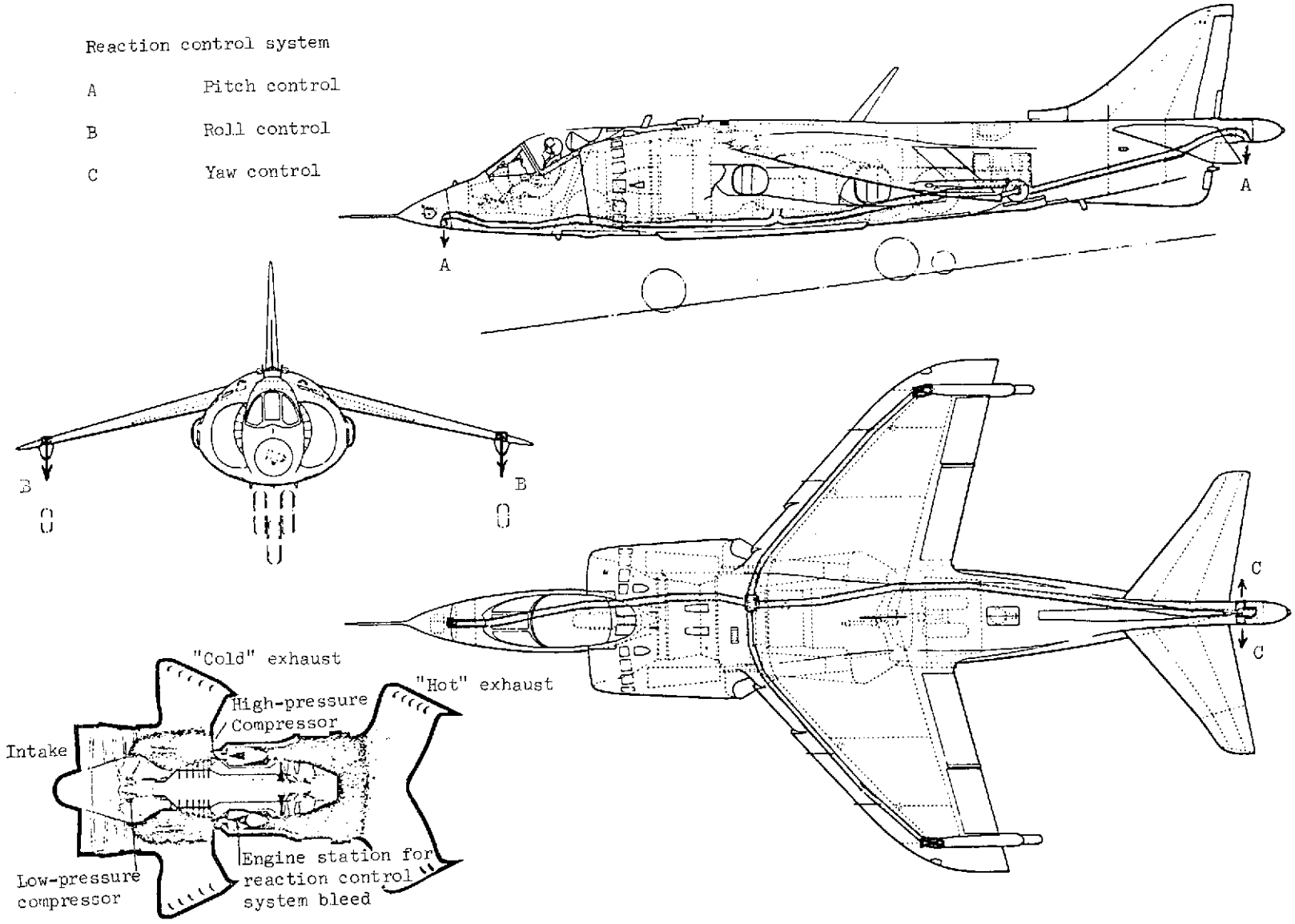

Figure 1.- Three-view drawing of test aircraft showing reaction control system and sketch of thrust-vectoring system.

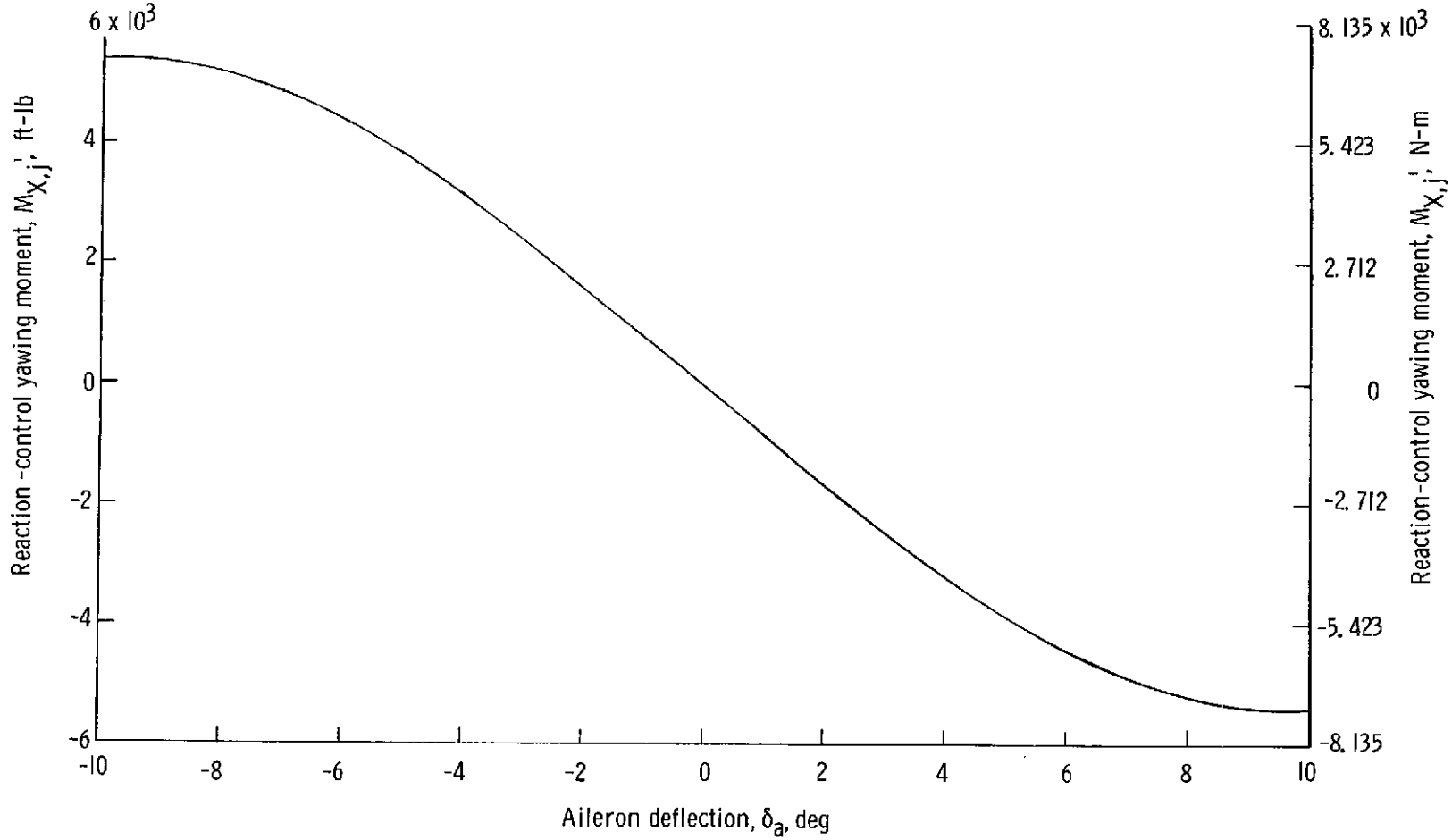

Figure 2.- Variation in reaction-control rolling moment with aileron deflection. Values of $M_{X,j}'$ taken from manufacturer's report.

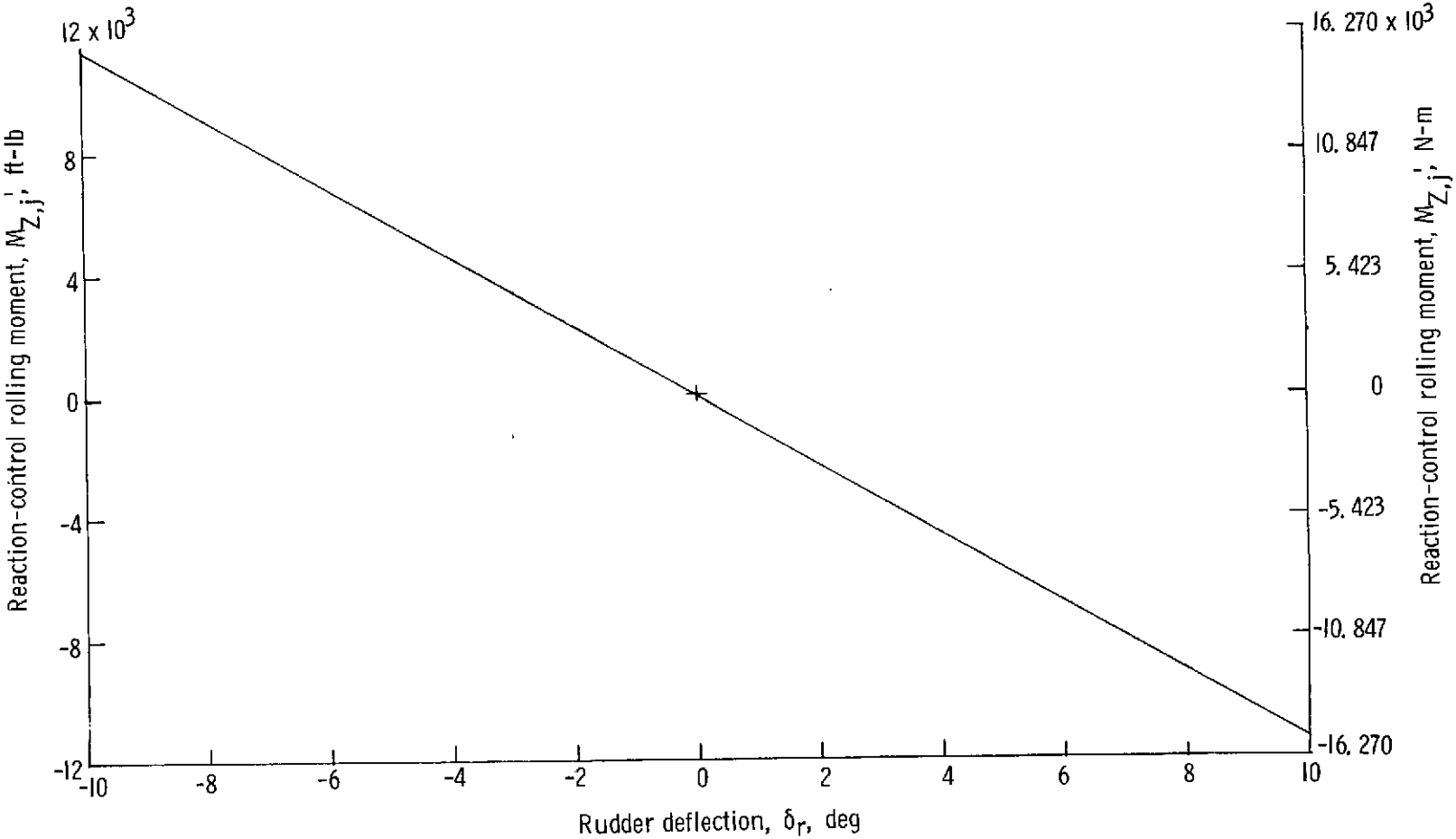

Figure 3.- Variation in reaction-control yawing moment with rudder deflection. Values of $M_{Z,j}'$ taken from manufacturer's report.

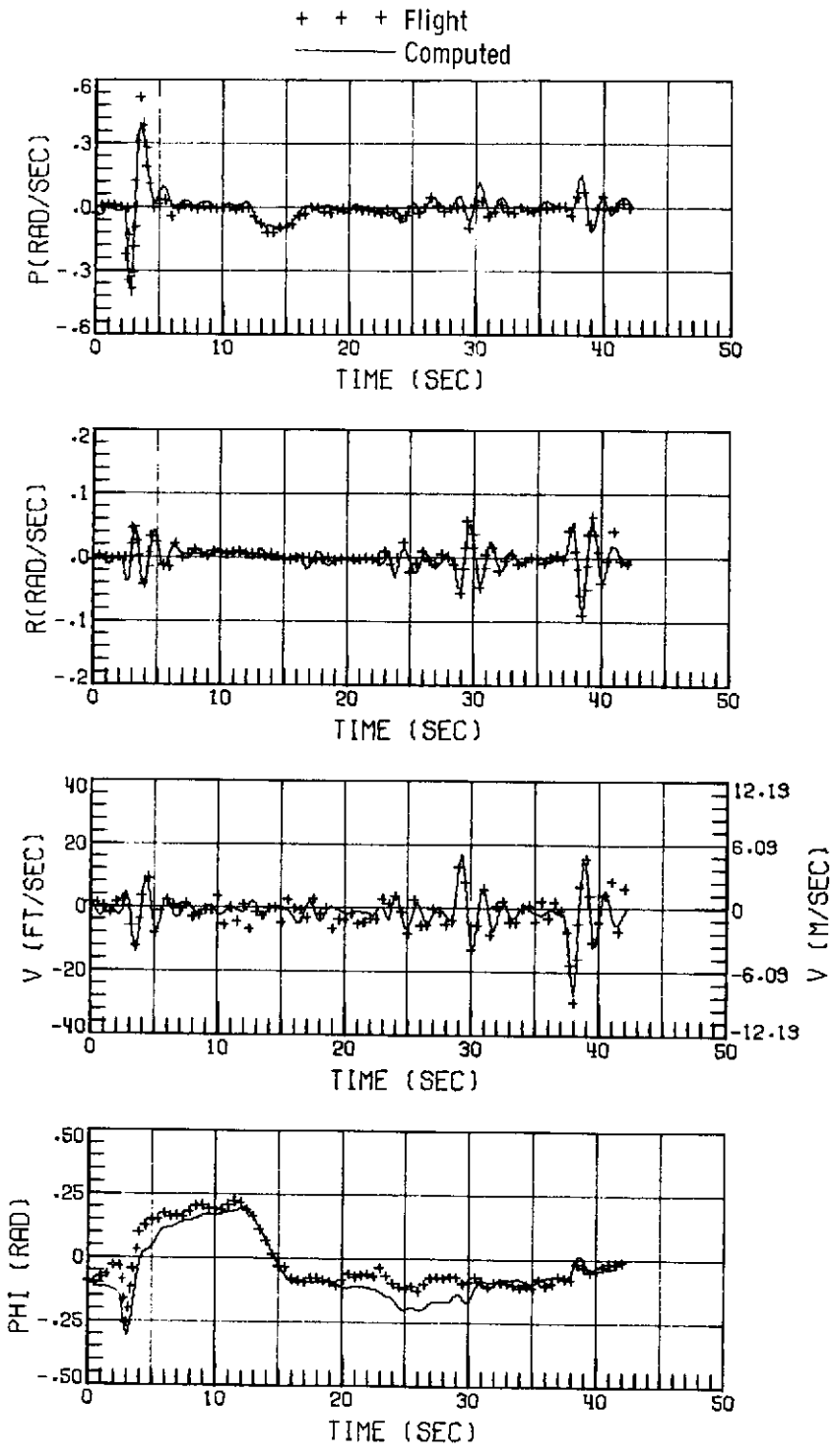

(a) $\theta_j = 0^o$.

Figure 4.- Comparison of flight data with time histories computed by using aerodynamic parameters of table V; Mach number, 0.82.

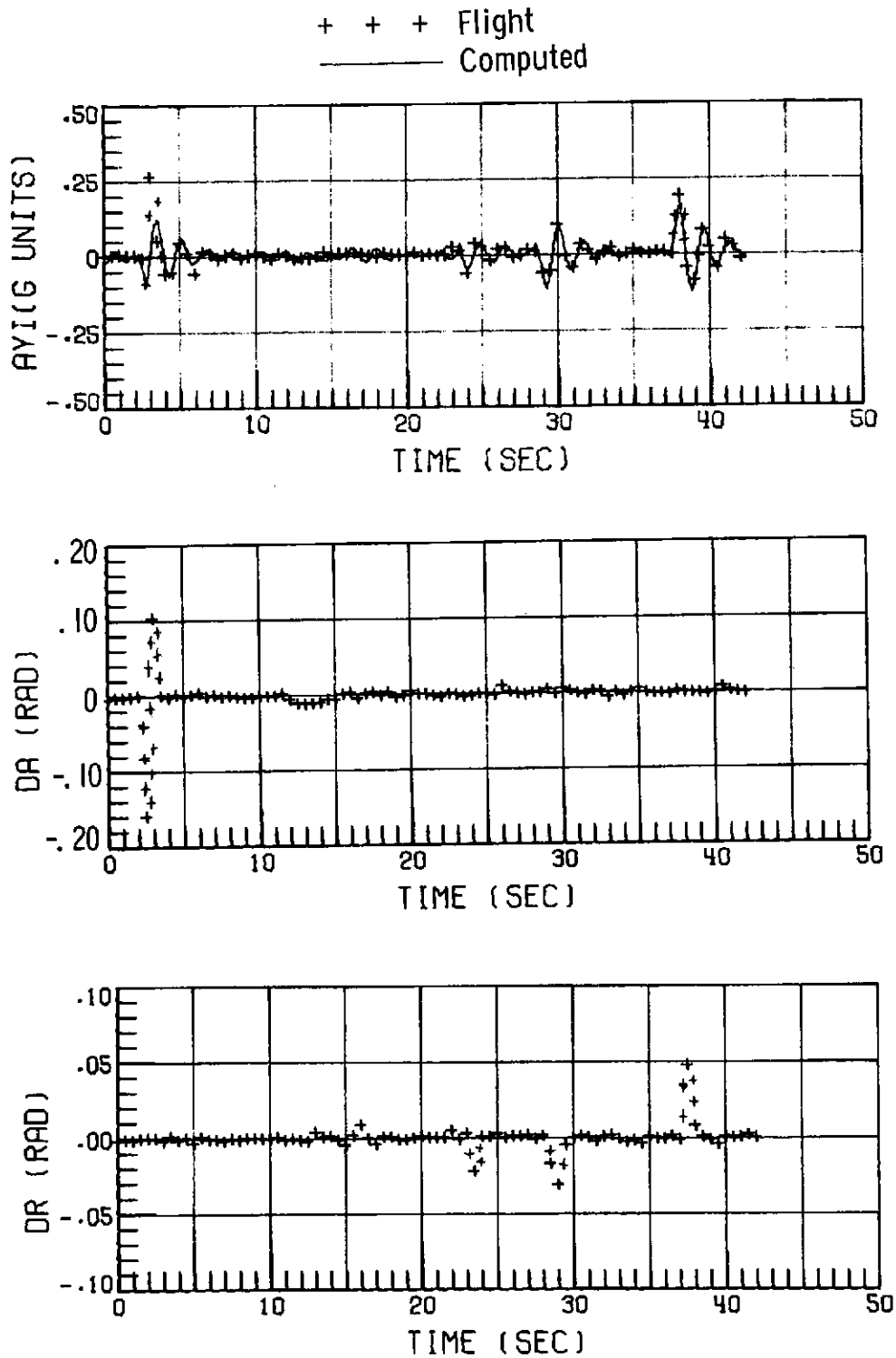

(a) $\theta_j = 0^o$. Concluded.

Figure 4.- Continued.

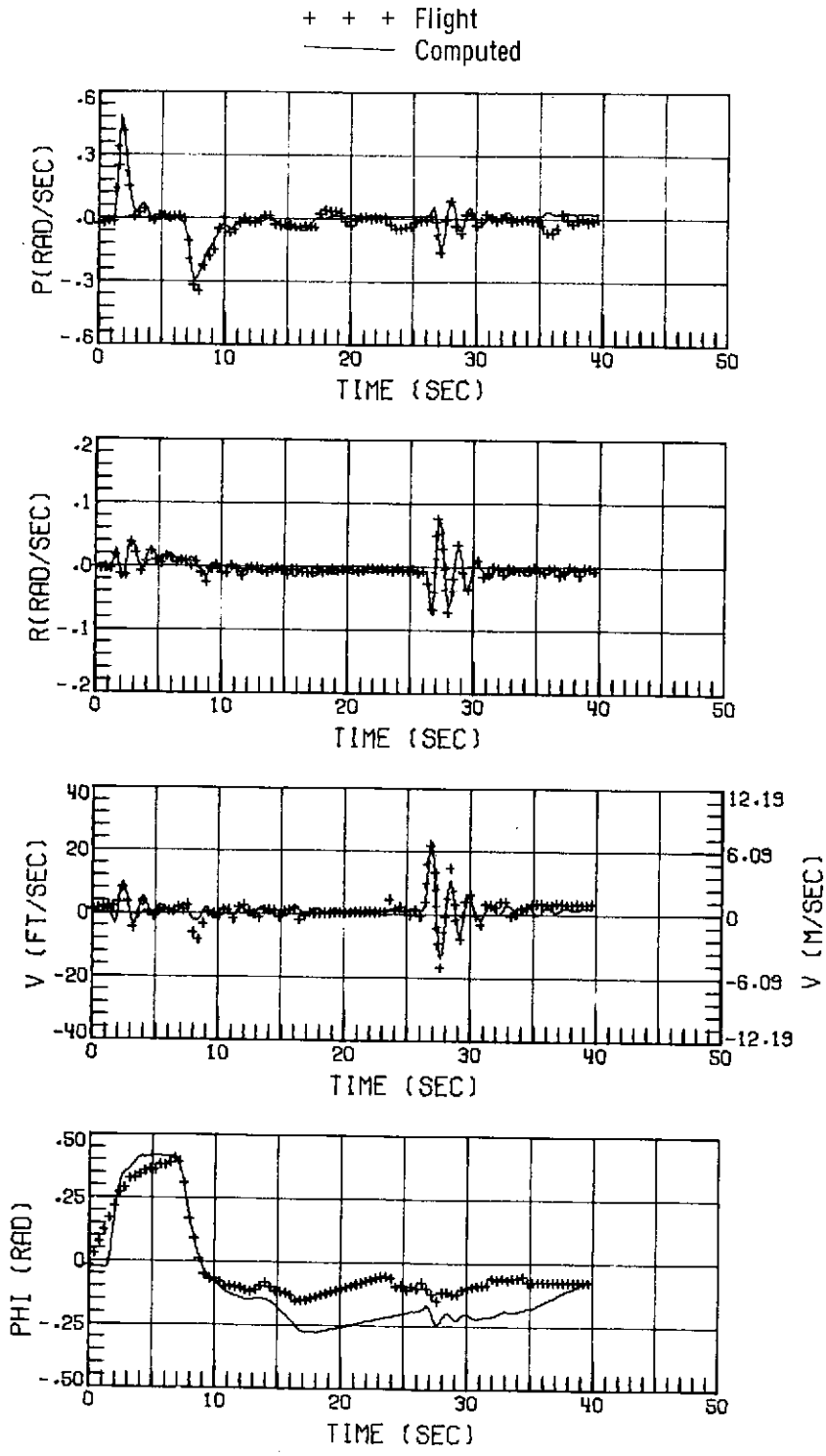

(b) $\theta_j = 15^o$.

Figure 4.- Continued.

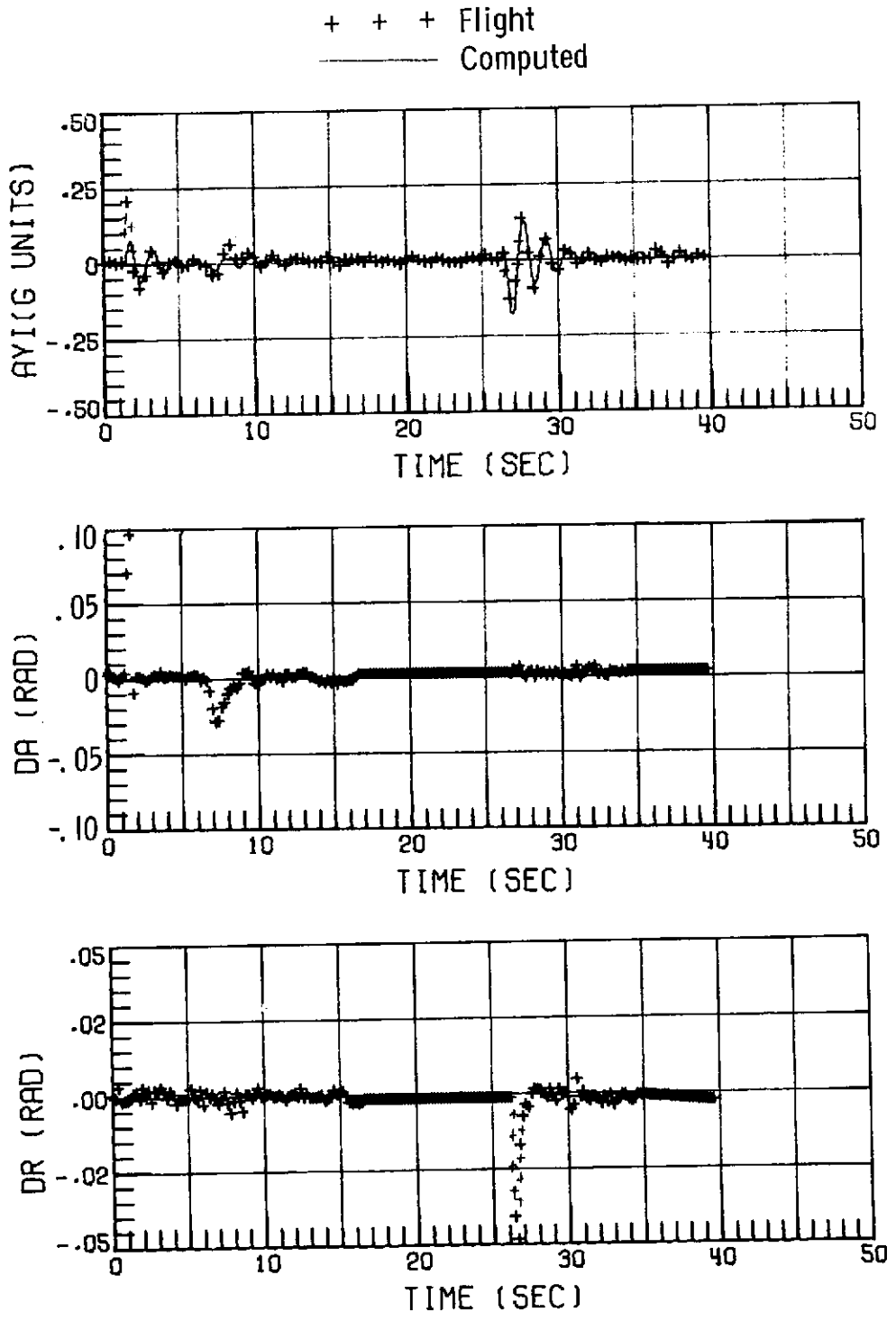

(b) $\theta_j = 15^o$. Concluded.

Figure 4.- Continued.

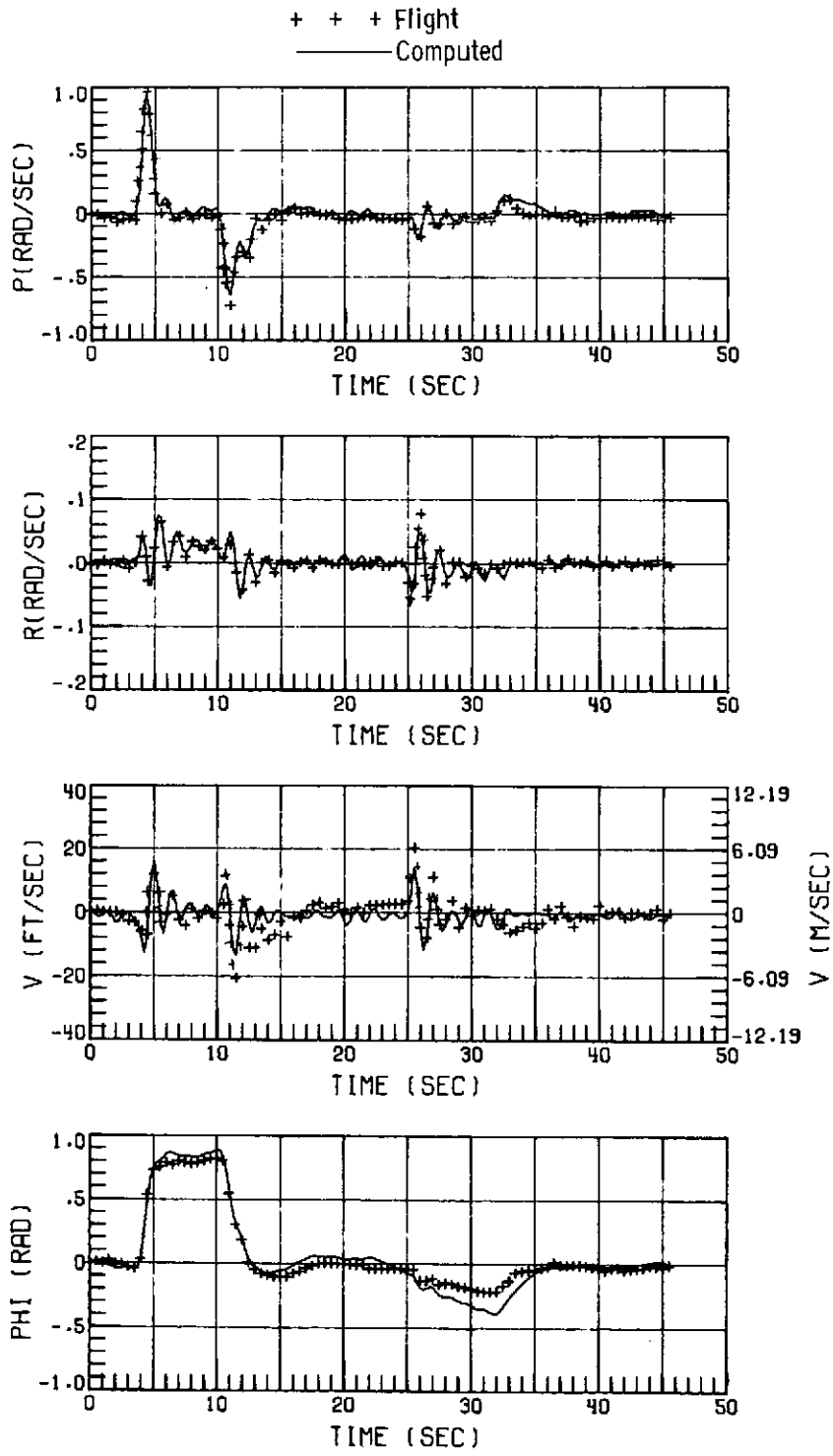

(c) $\theta_j = 30^o$.

Figure 4.- Continued.

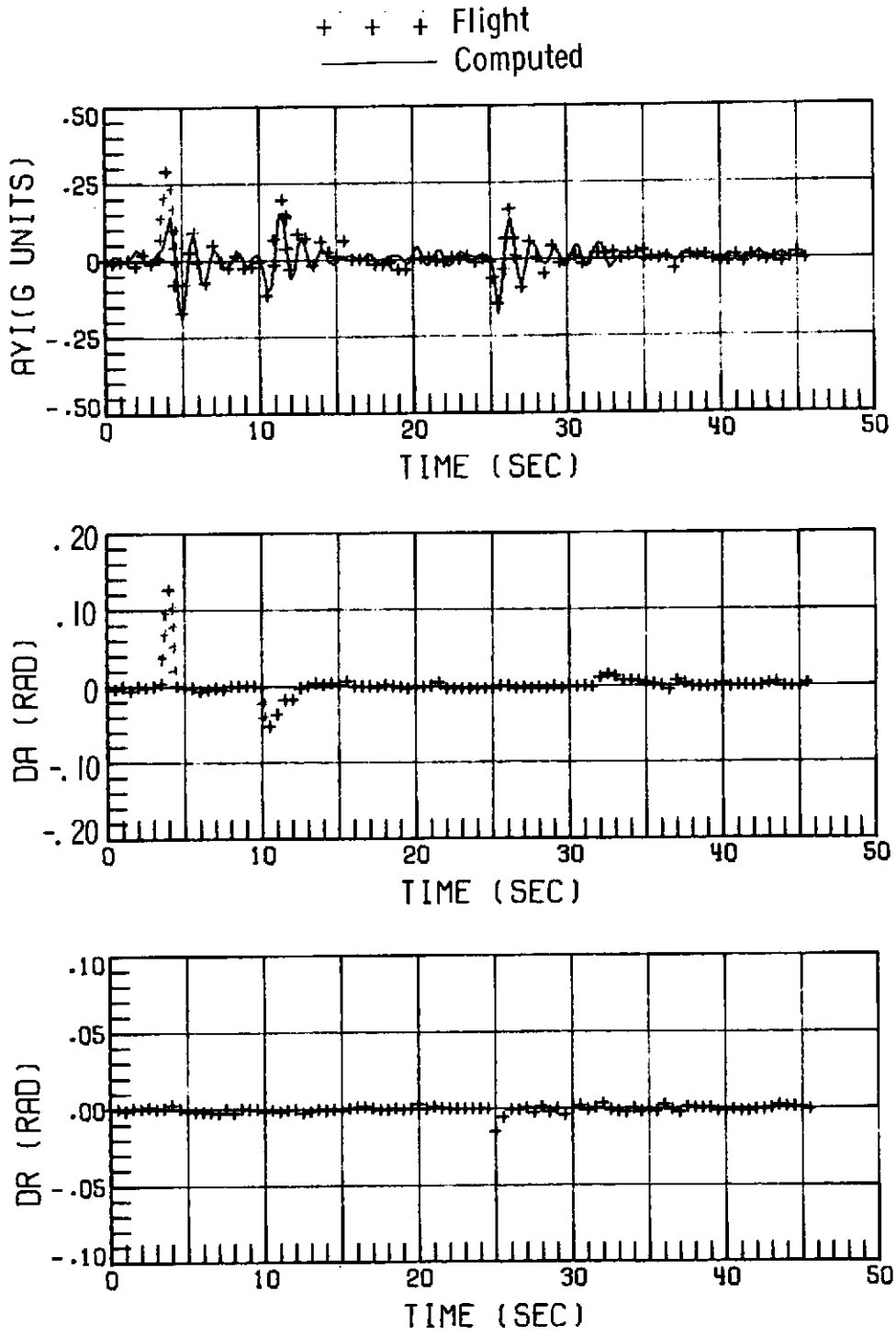

(c) $\theta_j = 30^o$. Concluded.

Figure 4.- Concluded.

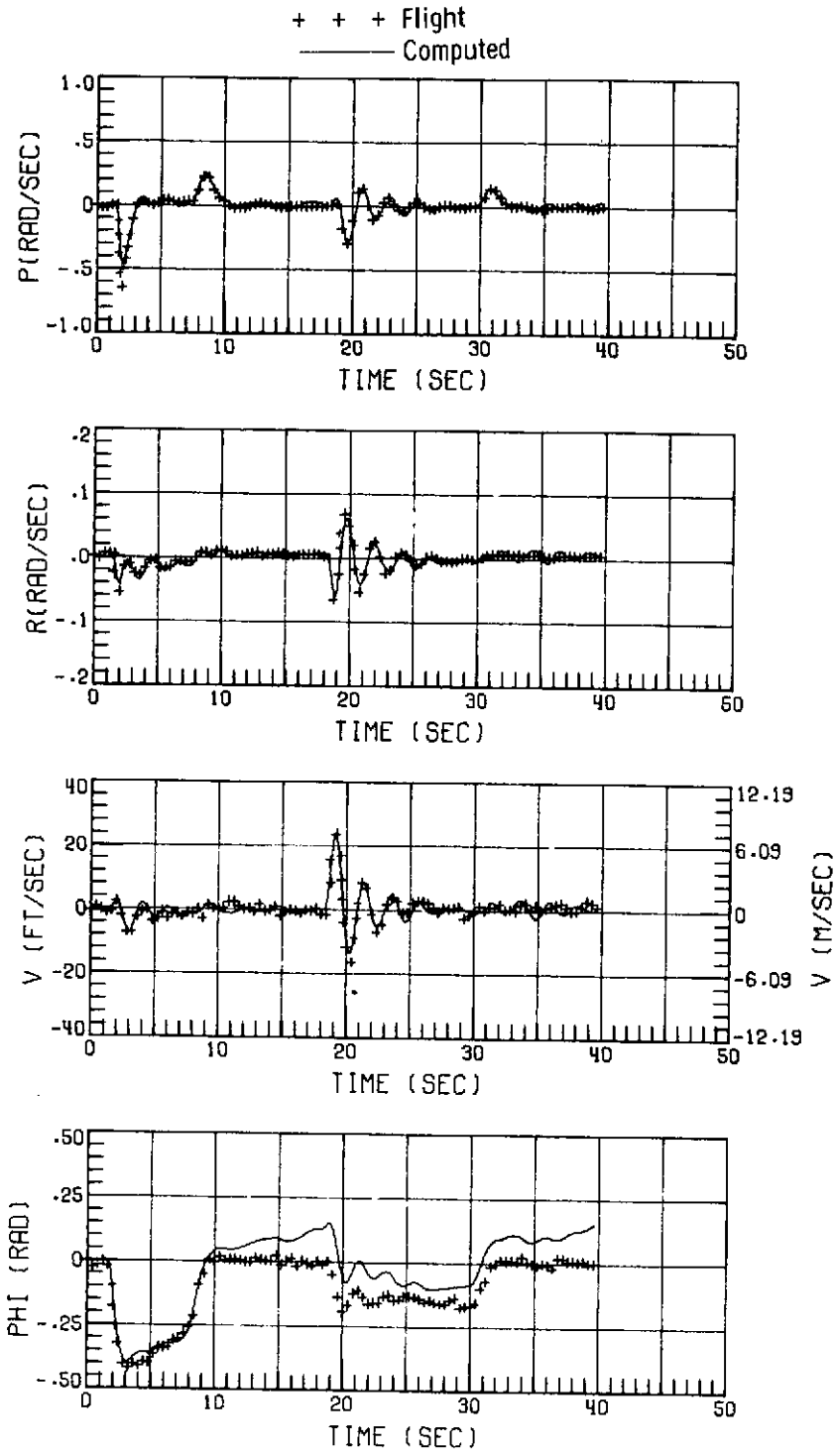

(a) $\theta_j = 0^o$.

Figure 5.- Comparison of flight data with time histories computed by using aerodynamic parameters of table V; Mach number, 0.62.

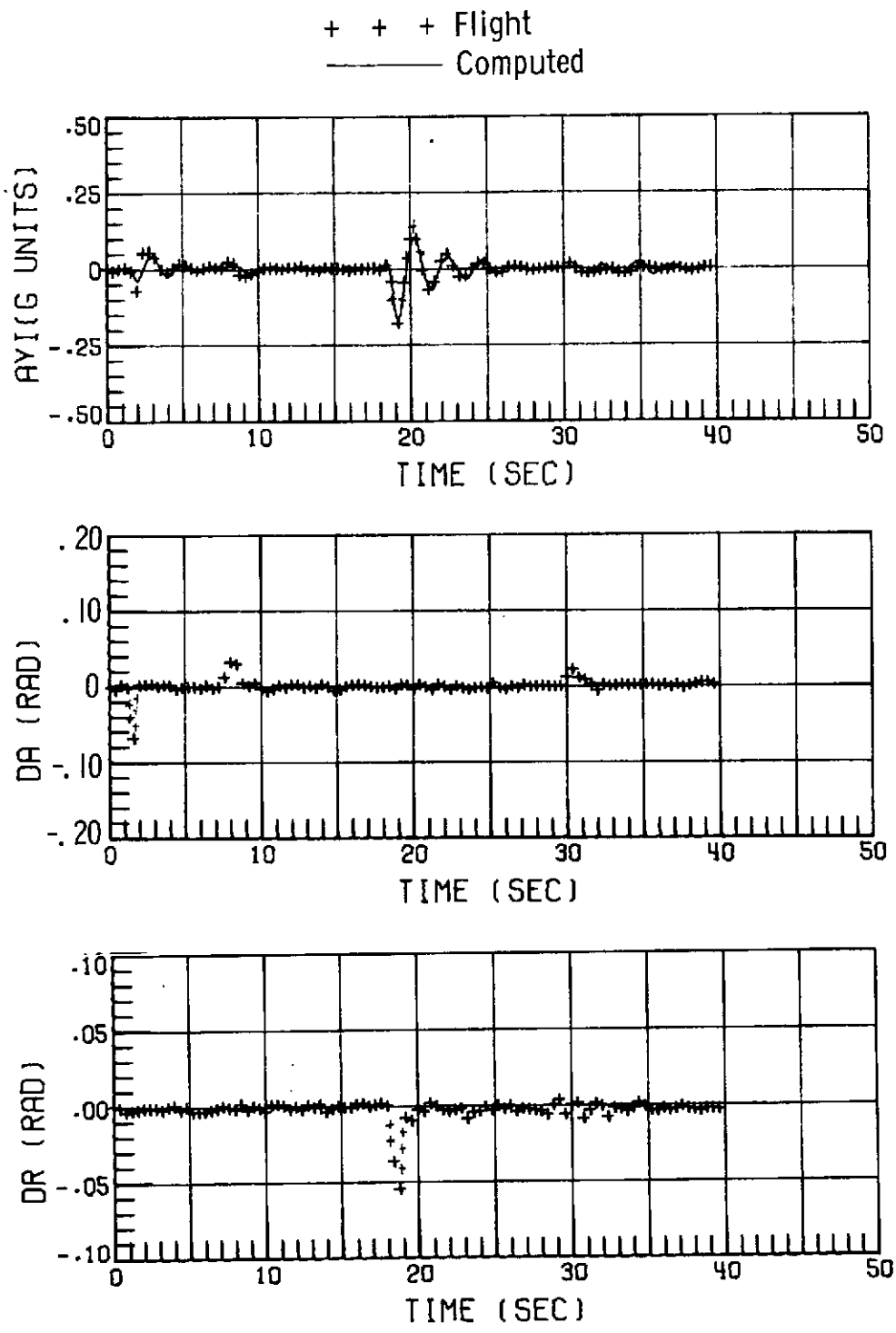

(a) $\theta_j = 0^o$. Concluded.

Figure 5.- Continued.

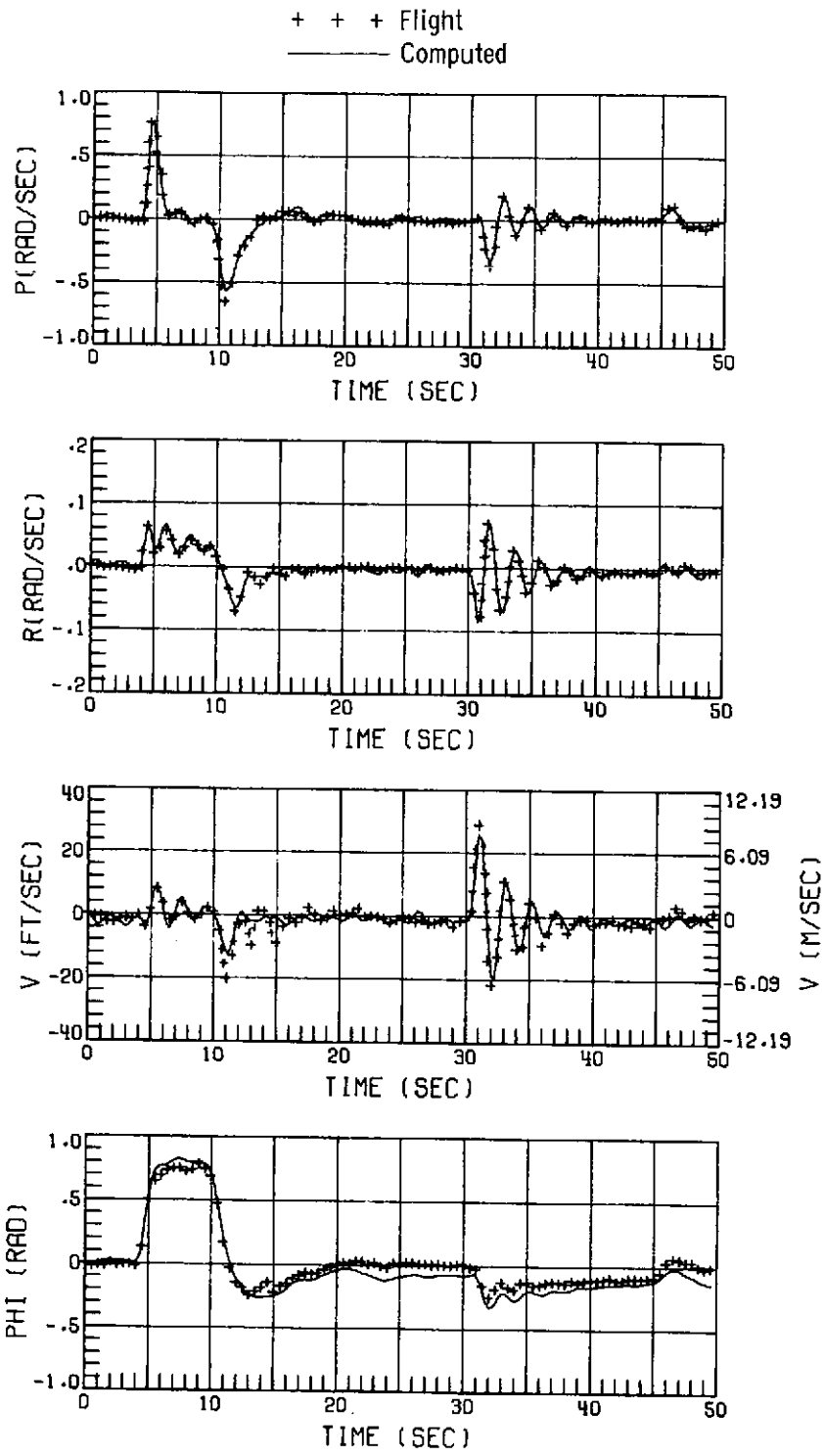

(b) $\theta_j = 15^o$.

Figure 5.- Continued.

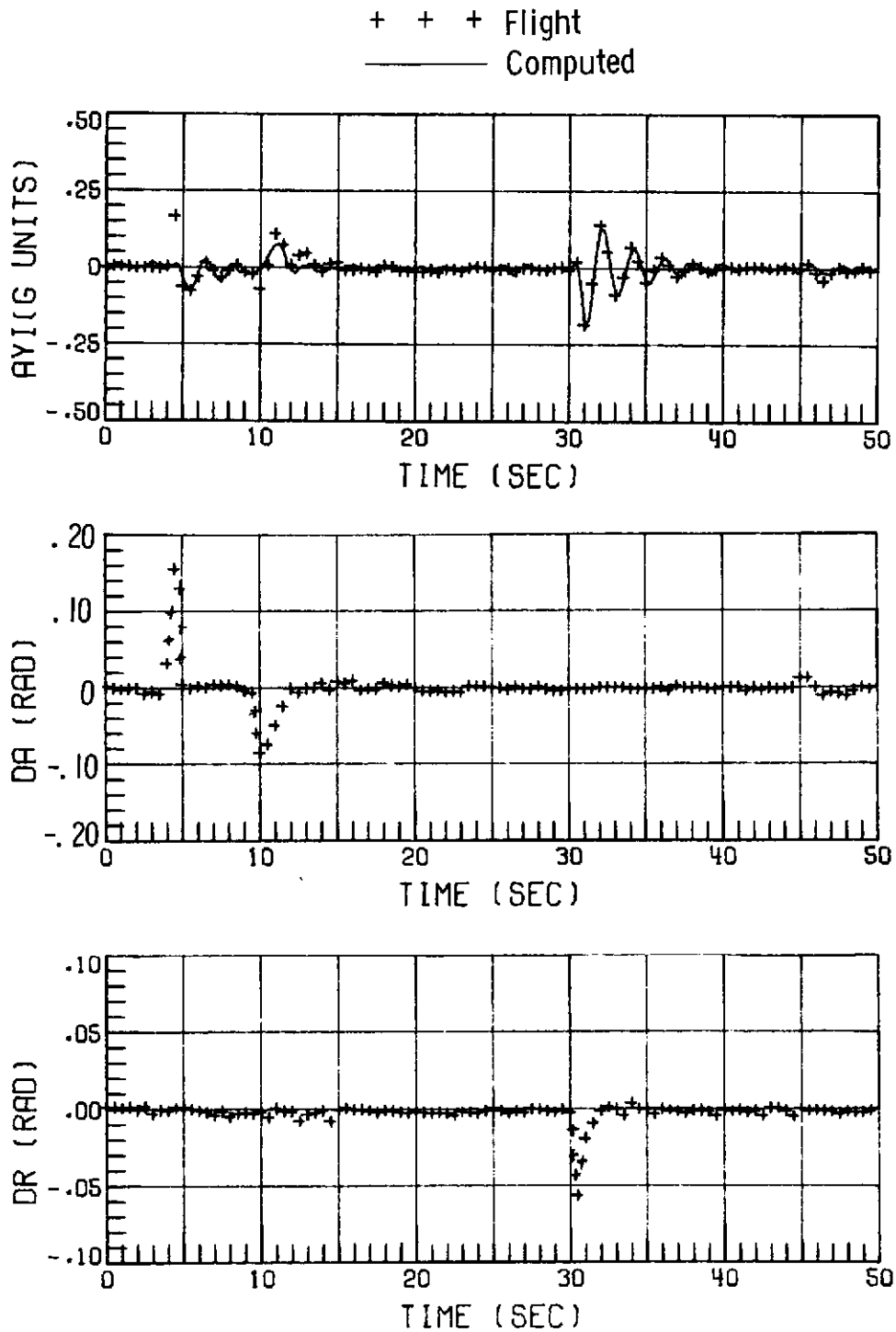

(b) $\theta_j = 15^o$. Concluded.

Figure 5.- Concluded.

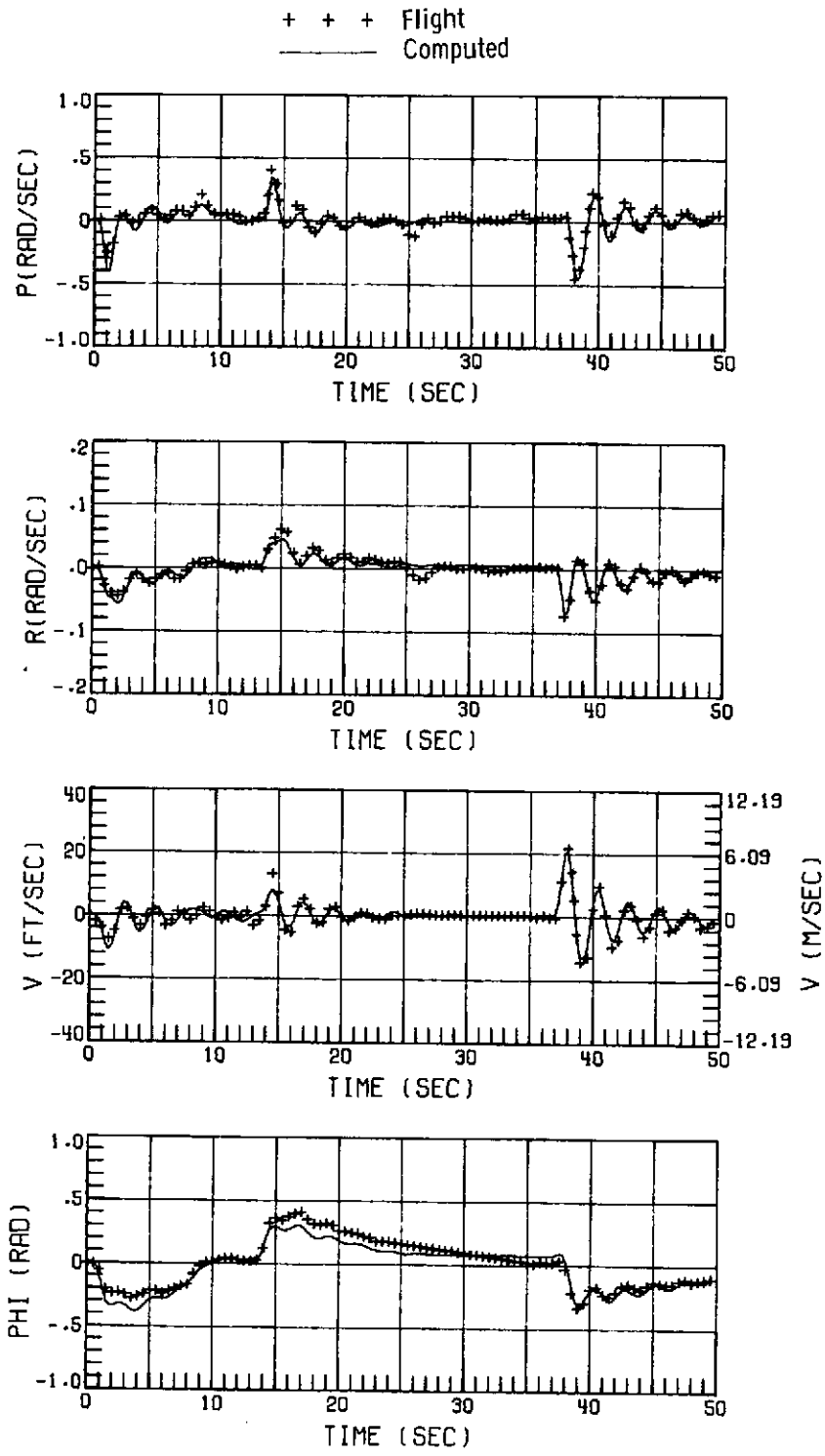

(a) $\theta_j = 0^o$.

Figure 6.- Comparison of flight data with time histories computed by using aerodynamic parameters of table V; Mach number, 0.43.

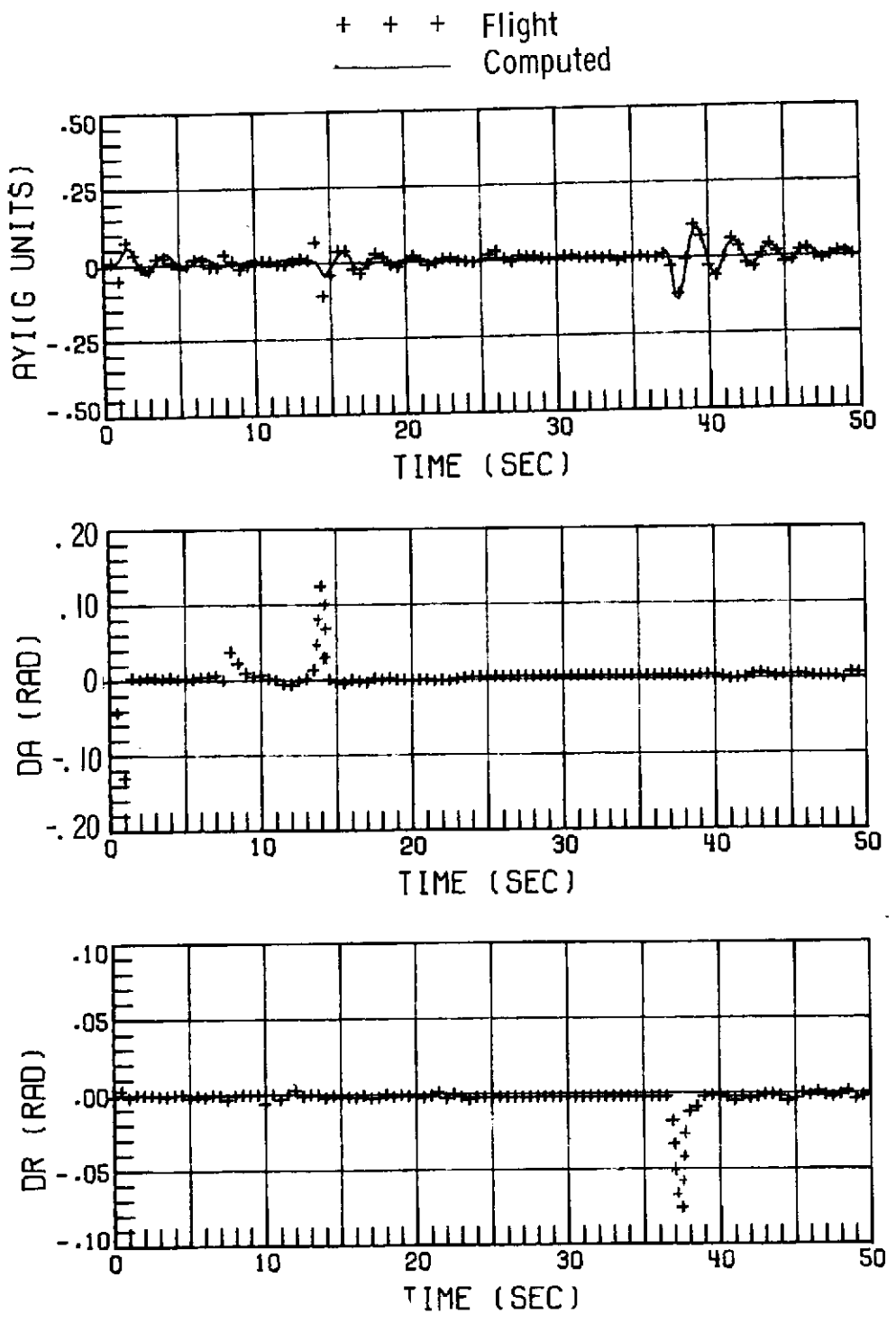

(a) $\theta_j = 0^o$. Concluded.

Figure 6.- Continued.

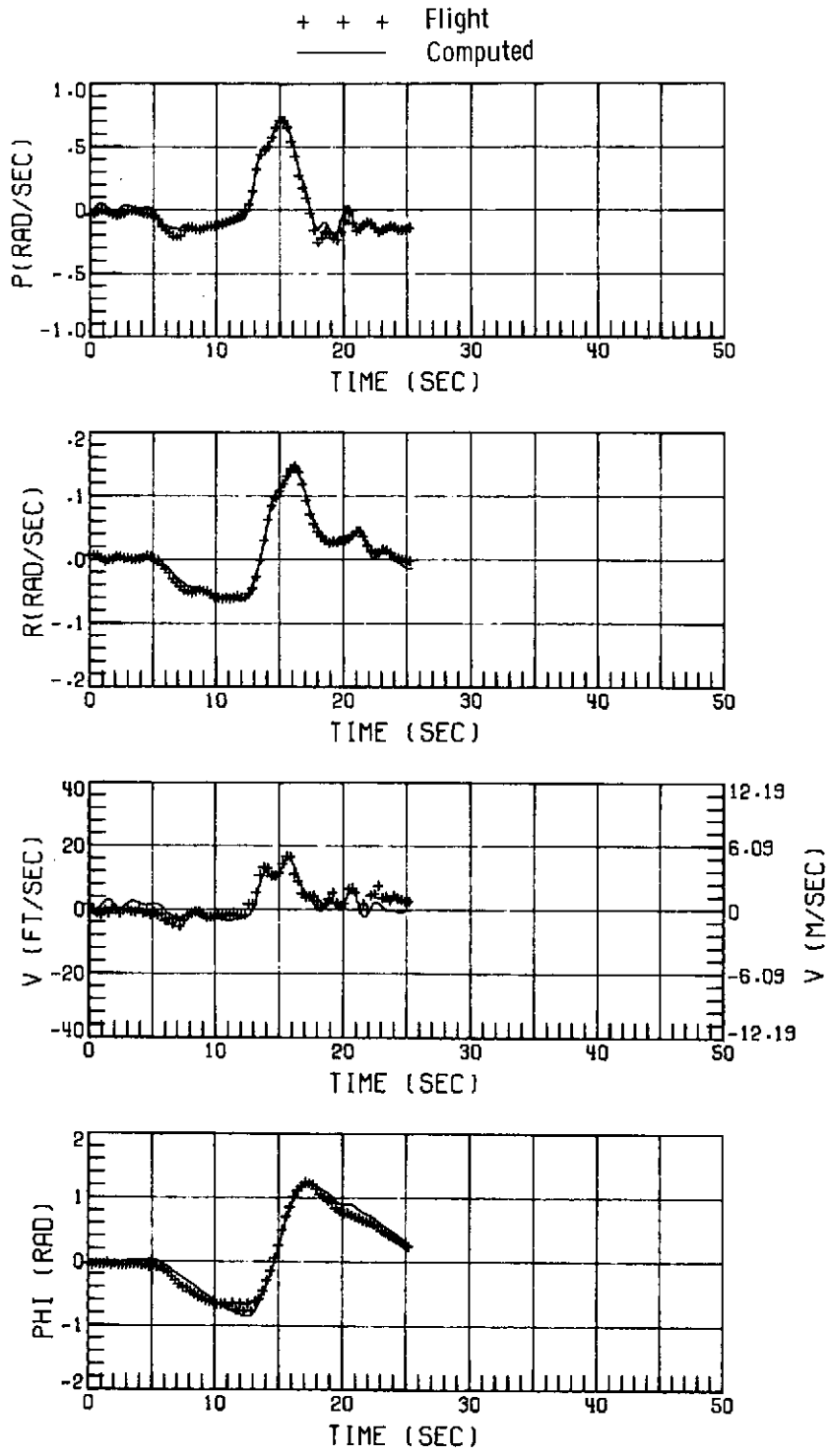

(b) $\theta_j = 15^o$.

Figure 6.- Continued.

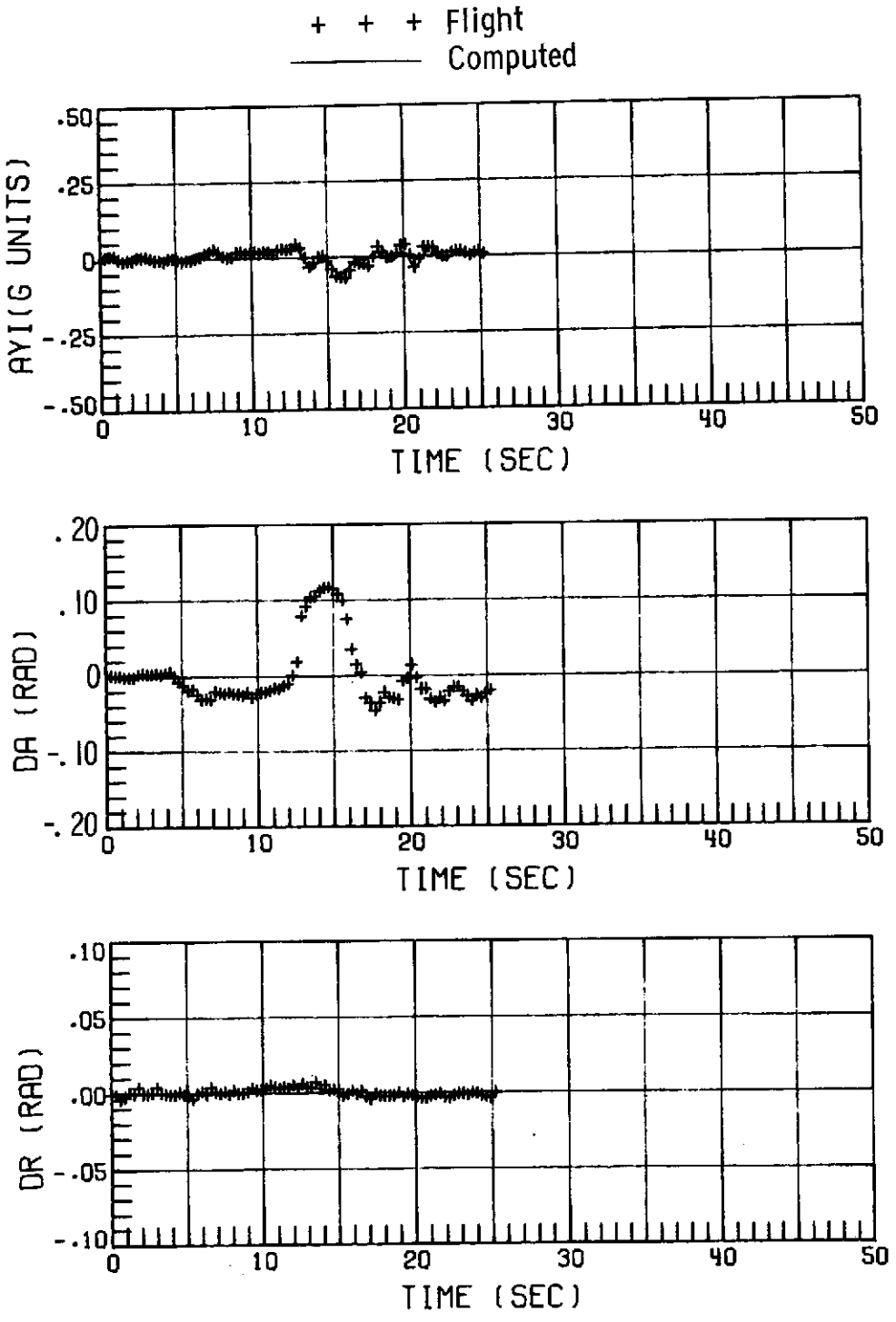

(b) $\theta_j = 15^o$. Concluded.

Figure 6.- Continued.

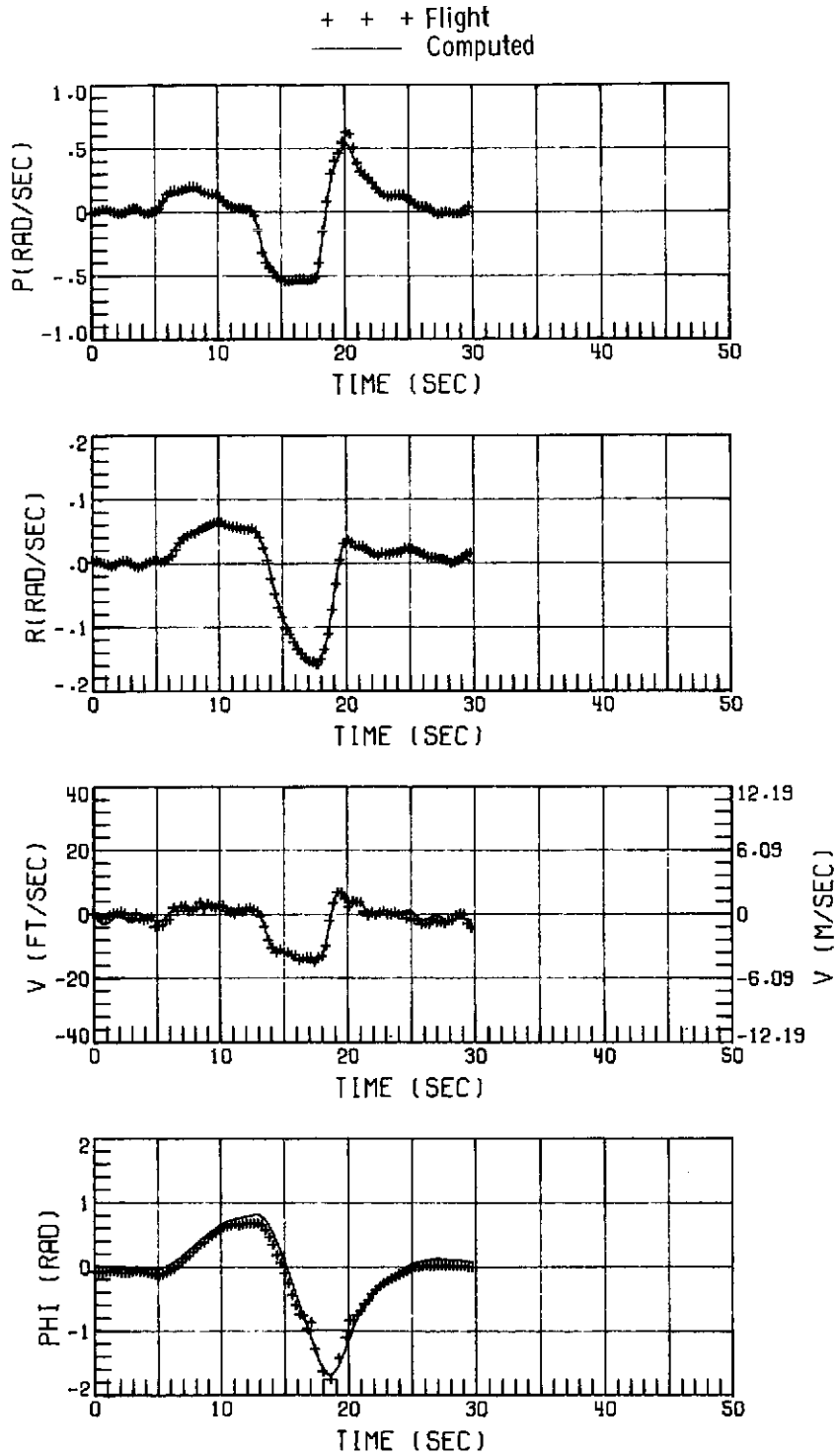

(c) $\theta_j = 30^o$.

Figure 6.- Continued.

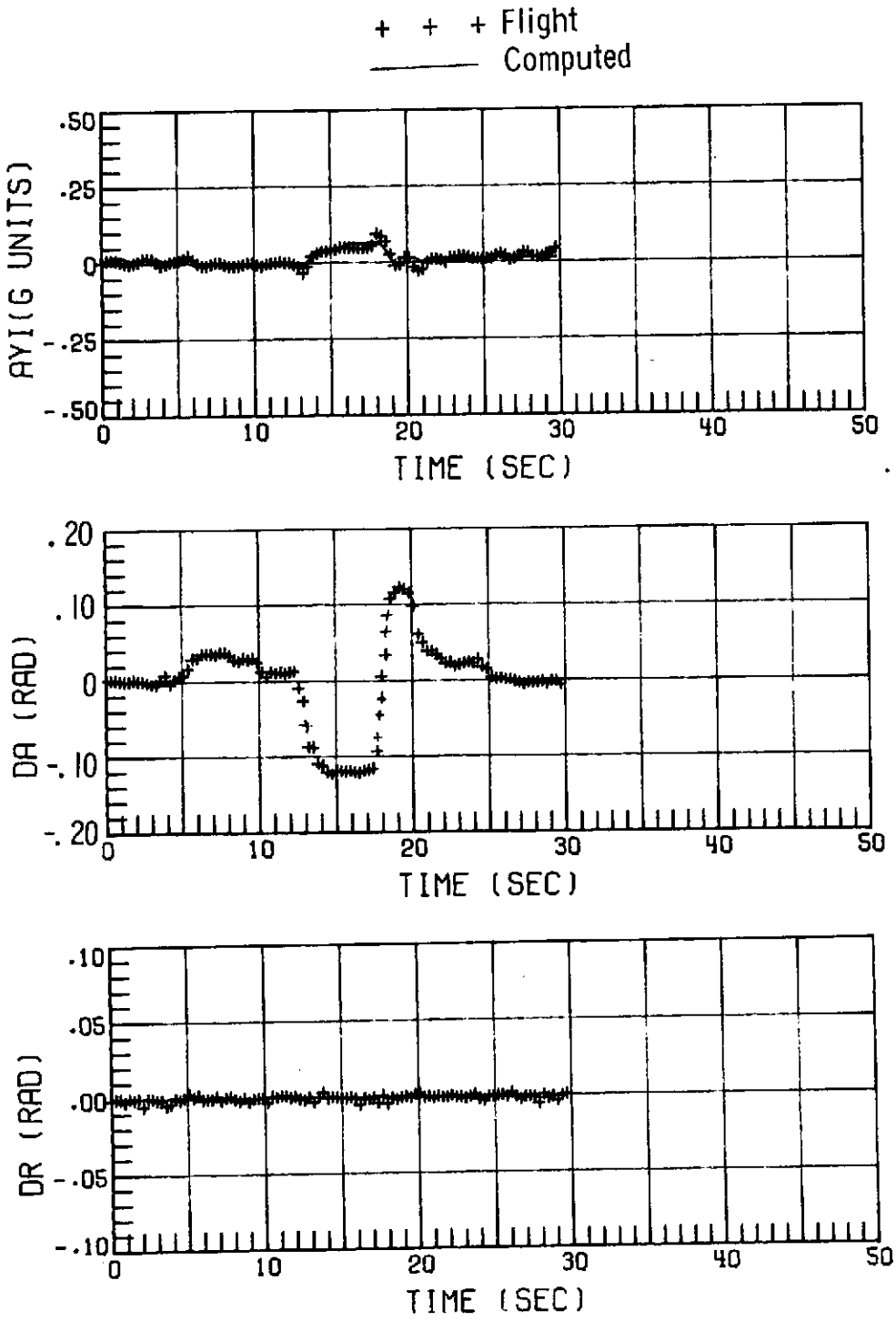

(c) $\theta_j = 30^o$. Concluded.

Figure 6.- Concluded.

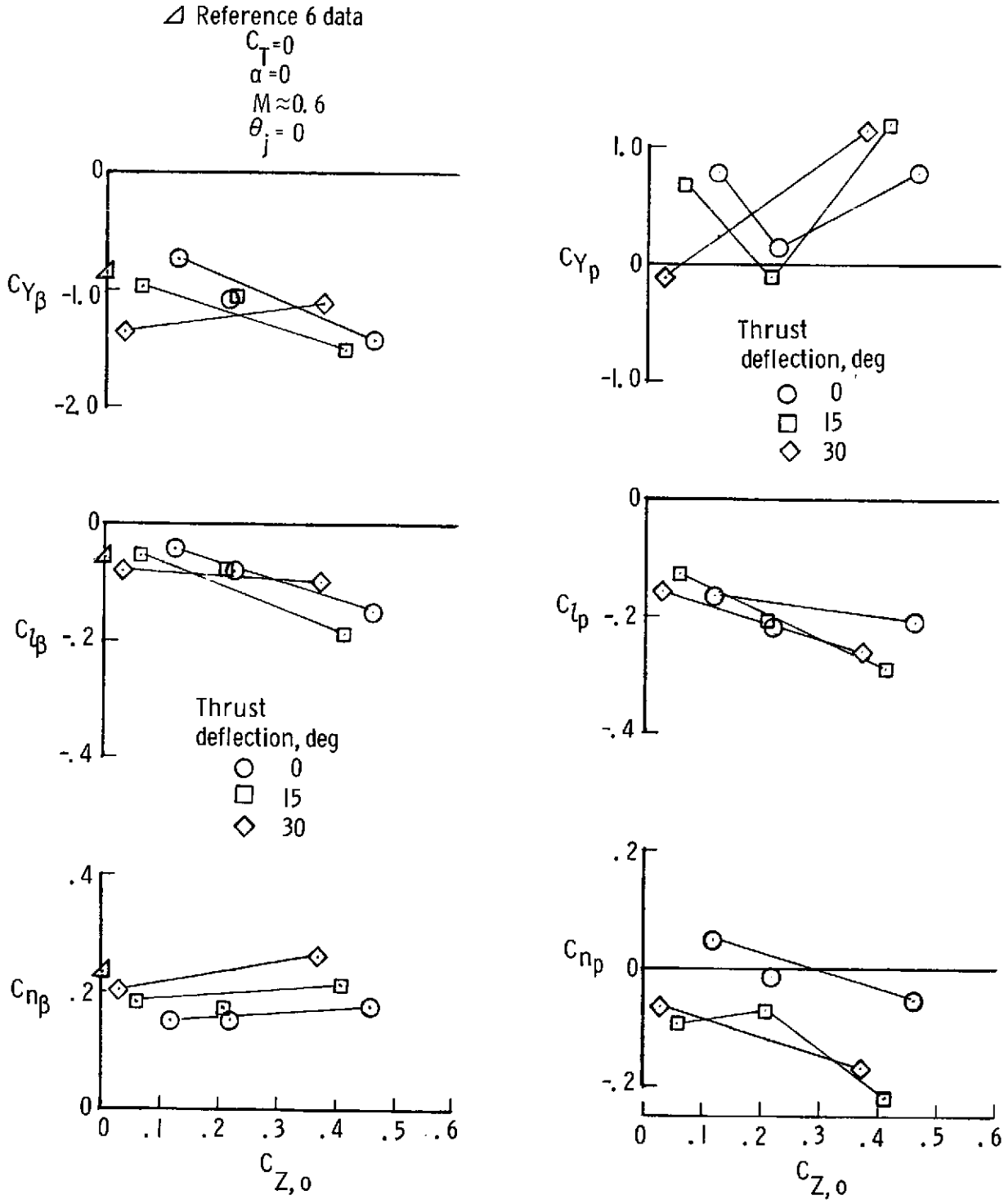

(a) Sideslip derivatives.

(b) Rolling derivatives.

Figure 7. Various lateral aerodynamic derivatives plotted against trim-normal-force coefficient.

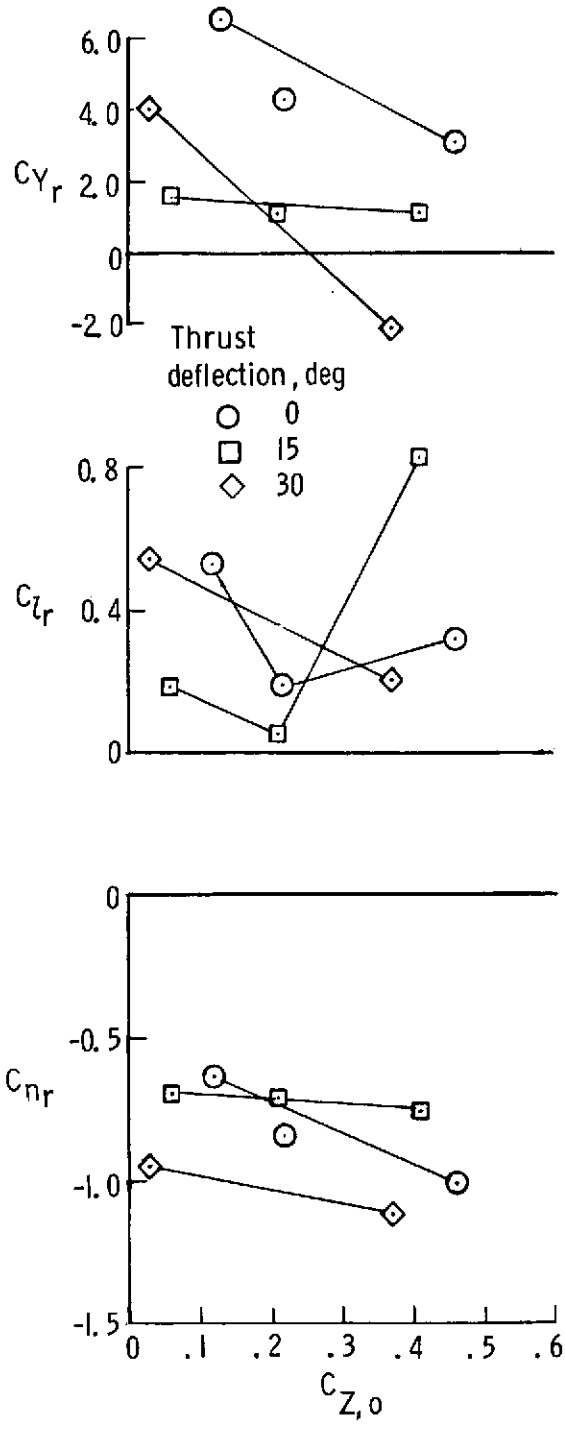

(c) Yawing derivatives.

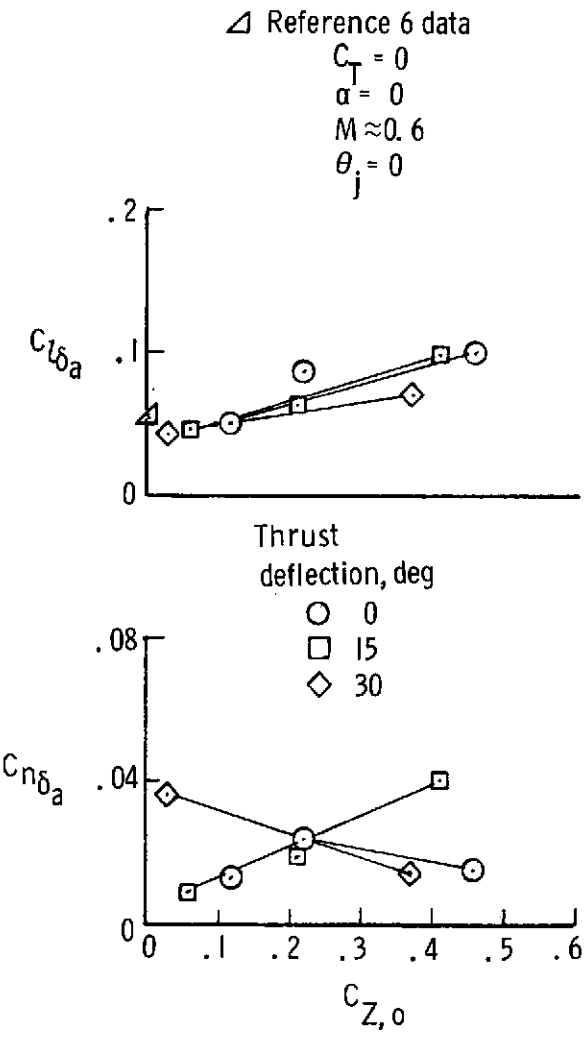

(d) Aileron parameters.

Figure 7.- Continued.

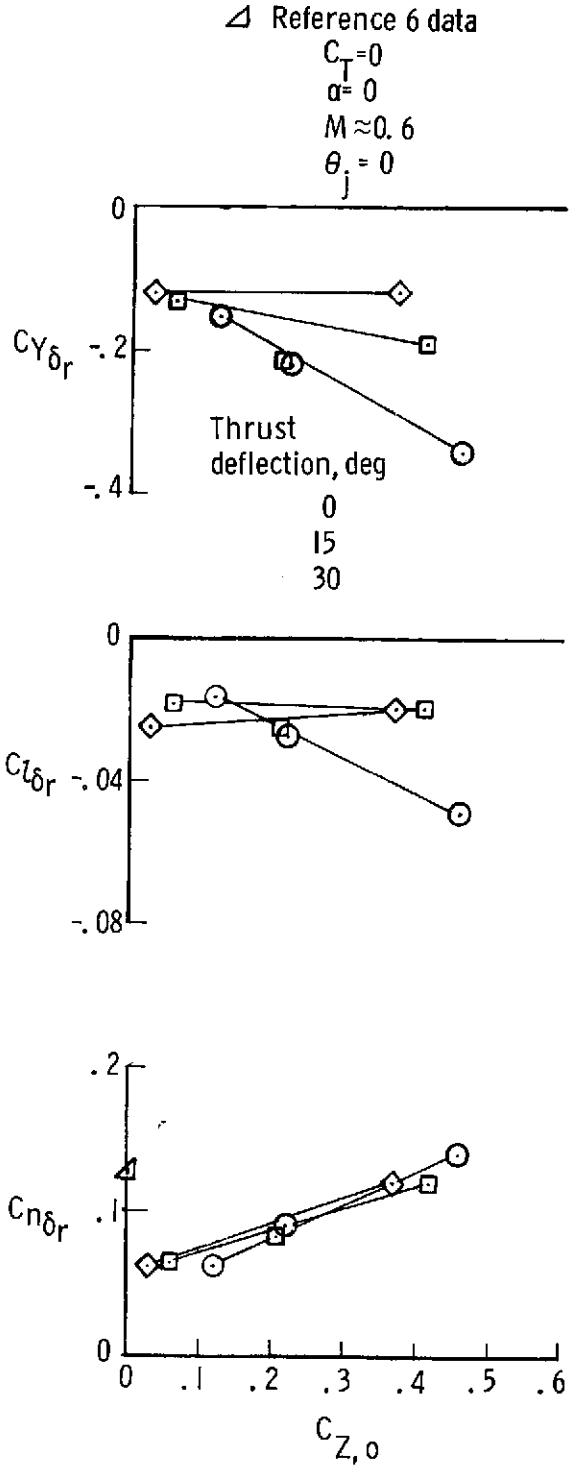

(e) Rudder parameters.

Figure 7.- Concluded.

NASA-Langley, 1974 L-9176